Nanotube- and Nanorod-Based Dye-Sensitized Solar Cells

Yung-Eun Sung, Soon Hyung Kang and Jae-Yup Kim

Abstract Considerable efforts have been devoted to the design and synthesis of low-dimensional, nanostructured materials due to their morphology-dependent performances. In particular, one-dimensional (1-D) TiO_2 nanostructures, including nanorods (NRs), nanowires (NWs), and nanotubes (NTs), have attracted considerable interest due to their unique characteristics. In dye-sensitized solar cell (DSSC) operation, 1-D nanostructure-based photoanodes can contribute to rapid electron transport, ensuring efficient charge collection by the conducting substrate in competition with recombination. Relying on the ordering of 1-D TiO_2 nanomaterial, the conversion efficiency of DSSCs was affected because electron collection is determined by trapping/detrapping events at the site of the electron traps, such as defects, surface states, grain boundaries, and self-trapping. This point has promoted research on self-ordered, 1-D photoanodes stretched on a substrate with enhanced electron transport properties due to their desirable features: highly decreased intercrystalline contacts and a structure with a specified directionality. In this literature review, the preparation of various 1-D nanomaterials from disordered to ordered states and their electron dynamics in the application of DSSCs are reviewed.

Y.-E. Sung (✉)
World Class University (WCU) Program of Chemical Convergence for Energy & Environment (C2E2), School of Chemical & Biological Engineering, Seoul National University, Seoul 151-744, Korea
e-mail: ysung@snu.ac.kr

S. H. Kang
Department of Chemistry Education, Chonnam National University, Gwangju 500-757, Korea
e-mail: skang@jnu.ac.kr

J.-Y. Kim
School of chemical and Biological Engineering and Interdisciplinary Program in Nano Science and Technology, Seoul National University, Seoul 151-742, Korea

L. Zang (ed.), *Energy Efficiency and Renewable Energy Through Nanotechnology*, Green Energy and Technology, DOI: 10.1007/978-0-85729-638-2_9,

1 Introduction

Titanium dioxide (TiO_2) is a typical wide-band gap (3.2 eV) semiconductor that has been studied extensively in areas such as synthesis, deposition methods, crystal structure, optical properties, phase stability, photosensitivity,and morphological changes [1, 2]. In particular, among the various morphological phases, 1-dimensional (1-D) TiO_2 nanostructures such as nanorod (NR)/nanowire (NW) and nanotube (NT) have been widely investigated on account of their unique microstructure and promising features, such as a high-aspect-ratio, high surface area, higher surface area/volume ratio, increased number of delocalized carriers, and improved charge transport afforded by dimensional anisotropy with the conventional properties [3–5]. Their remarkable properties have led to their use in a variety of applications including dye-sensitized solar cells (DSSCs), photocatalysts,and photochromic devices [6, 7]. In particular, the DSSC is a photoelectrochemical cell that converts visible light energy into electricity and is considered an alternative to silicon solar cells due to its attainable high efficiency, environmental intimacy, and cost effectiveness.

Figure 1 shows the operating principle of a DSSC consisting of a semiconductor photoanode (electron transporting layer), dye (a photosensitizer), electrolyte containing I^-/I_3^- redox couples (an electron transfer mediator), and Pt-coated counter electrode (a catalyst for electron transfer). The DSSC features dye molecules chemisorbed onto the surface of a semiconductor nanocrystal filled with an electrolyte. Under light illumination, charge separation occurs at the dye/semiconductor interface, where photoexcited dyes inject electrons into the conduction band of the semiconductor, after which the original state of the dye is restored by electron donation from the electrolyte containing the I^-/I_3^- redox system. The iodide is regenerated, in turn, by reduction of triiodide at the counter electrode, with the circuit being completed through the external load. The theoretical maximum voltage under the illumination corresponds to the difference between the redox potential of the redox mediator and the Fermi level of the semiconductor photoanode. Along with these processes, as side reactions, electrons in the conduction band of the semiconductor may be recombined with the oxidized dye molecules or electron acceptor species from the electrolyte. Therefore, the following aspects of the photoanode deserve important consideration. Firstly, injected electrons diffuse through thousands of particles before they reach the transparent conductive oxide (TCO) substrate, emphasizing the importance of good electronic inter-particle connection. Furthermore, recombination plays a critical role because of the extremely large TiO_2/dye/electrolyte interface area and the proximity of electrons to the oxidized redox species (the hole carriers), which can limit the photovoltaic performance. In its original form, the DSSC used the mesoporous nanocrystalline TiO_2 film in replacement of the previous flat TiO_2 electrode to enhance the light-harvesting dye. Adsorption resulted from the highly expanded surface area, with a reported conversion efficiency of 7% [8]. Subsequently, to improve the conversion efficiency, both the size (<20 nm) and phase (anatase, rather than rutile) of the TiO_2 nanoparticles (NPs) were optimized. The TiO_2 film

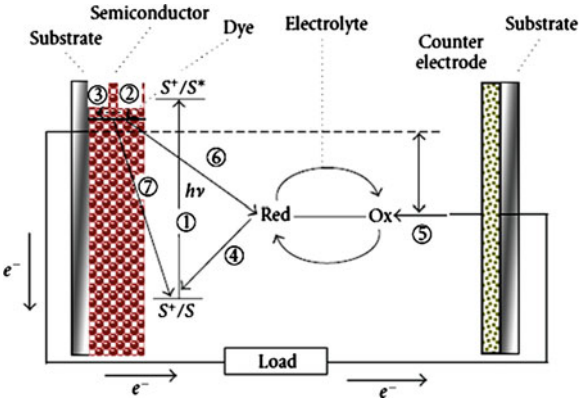

Fig. 1 Simple representation and operating principal of dye-sensitized solar cells (DSSCs)

thickness has a significant effect on the light-harvesting efficiency and charge recombination in that the conversion efficiency increases linearly with increasing TiO_2 thickness due to the increased dye uptake. However, above a limited thickness, the efficiency begins to degrade as a result of dominant charge recombination and mass transport limitations [9]. This is easily explained by the electron diffusion length in TiO_2 films, which is the distance that photoinjected electrons transport through a nanoporous network before reacting with the cations of the redox electrolyte in the DSSC system. In general, an electron diffusion length of approximately 15–20 μm in traditional electrodes composed of nano-sized TiO_2 particles (e.g., several orders of magnitude smaller than those in bulk single crystal TiO_2) is believed to limit the power conversion efficiency. This is because electron collection is determined by trapping/detrapping events along the site of the electron traps (defects, surface states, grain boundaries, self-trapping, etc.) [10, 11]. This point has focused research on photoanodes comprised of variously shaped nanoporous materials (rod, tube, wire, and tetra pad, etc.) with enhanced electron transport properties due to highly decreased intercrystalline contacts and structure with specified directionality. As a result, various methods for synthesizing 1-D TiO_2 particles have been reported [12–14].

However, the preparation of 1-D TiO_2 nanomaterials strongly influences their peculiar properties due to their enhancement or retardation in the fabrication process of the photoanode layer for DSSCs. Figure 2 shows the simple scheme to describe the disordered and ordered state of 1-D nanomaterials on the TCO substrate for the application of DSSCs. The disordered state of 1-D nanomaterial-based photoanode also provides additional grain boundaries or trapping sites, while the ordered state of 1-D nanomaterial-based photoanode shows straight electron percolation.

Herein, several approaches to prepare disordered (surfactant assisted, oriented attachment, sol–gel reaction, and hydrothermal process) and ordered (electrochemical anodization and hydrothermal process) 1-D TiO_2 nanomaterials and their electron dynamic properties for the application of DSSCs are summarized.

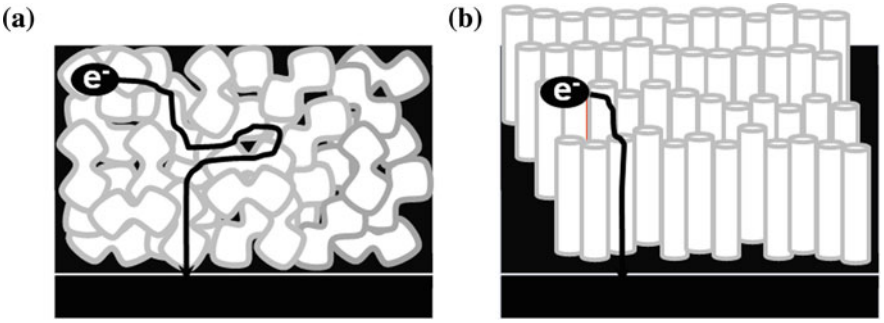

Fig. 2 Simple scheme to describe the ordered **a** and disordered **b** states of 1-D nanomaterials based on photoanode in the DSSCs

2 Preparation of Randomly Oriented TiO_2 Nanorod and Nanotube Films for Dye-Sensitized Solar Cells

NR-shaped TiO_2 nanocrystals are believed to have exceptional properties and have been considered an alternative to NPs. NRs have a higher surface area-to-volume ratio than NPs, thereby supplying a higher density of active sites for surface reactions as well as a high interfacial charge carrier transfer rate. Furthermore, increased delocalization of carriers in rods, where they can move freely throughout the length of the NRs, is expected to reduce the e^-/h^+ recombination probability. However, this is partially compensated by the traps in the surface sites to ensure more efficient charge separation [15]. Finally, NRs can potentially improve charge transport in the photoanodes of DSSCs when an ordered orientation of 1-D inorganic electron transporters is employed. Therefore, NRs offer direct electrical pathways for photogenerated electrons and can increase the electron transport rate, which in turn may improve the performance of DSSCs. Accordingly, a photoanode composed of 1-D TiO_2 NRs is a promising approach to which the following methodologies for synthesizing anisotropic TiO_2 nanomaterials have been applied: surfactant-assisted methods, oriented attachment, sol–gel reactions, and hydrothermal reactions.

2.1 Surfactant-Assisted Method

As a stabilizing agent, surfactants prevent aggregation of synthesized NPs and control their size and shape. With a large excess of surfactant, such as oleic acid, lateral expansion of the crystal lattice must be suppressed to achieve anisotropic crystal growth [16]. Oleic acid plays two roles: stabilizing solvent and chemical modifier to control the hydrolysis rate of the precursor. For better tuning of the growth rate of the different planes and control over the shape evolution of the anatase nanocrystals, the use of mixture surfactants that selectively bind to different crystal faces,and elimination of high-energy facets has been encouraged.

In this method, rod formation is usually realized when the surface free energies of the various crystallographic planes differ significantly. The use of different surface ligands that bind selectively to specific surface planes has been demonstrated as a suitable approach for rod formation in a controlled manner. As a representative example, Weller et al. reported the controlled growth of TiO_2 nanocrystals by modulation of the hydrolysis rate, using oleic acid as a stabilizing surfactant at 80°C [17]. In the present study, oleic acid served as an adsorbing-chelating ligand, restricting the growth rate along some crystallographic directions.

Moreover, the chemical modification of titanium alkoxide has been proven as a reasonable strategy to tune the reactivity of the precursor to water, manipulating the nanocrystal's growth kinetics and providing shape control over the resulting NPs. This synthetic route is a unique tool for easily functionalizing the TiO_2 nanocrystals surface with different capping ligands. Furthermore, Alivisatos's group reported a surfactant-mediated shape evolution of TiO_2 anatase nanocrystals in non-aqueous media. By using a surface selective surfactant, such as carboxylic acid, which binds strongly to the anatase (001) facets, modulation of the surface energies of the different crystallographic faces controlled the shape [18].

Recently, the Adachi group reported DSSCs using hydrothermally synthesized, single-crystalline TiO_2 NRs with diameters of 20–30 nm and lengths greater than 100 nm [19]. They synthesized TiO_2 NRs using selective surfactants, since the highest-energy facets were eliminated during crystal growth so that the progressive addition of a selective surfactant yielded a sequence of shapes. In the case of TiO_2 anatase, nucleation formed truncated octagonal bi-pyramidal seeds, exposing eight equivalent (101) faces and two equivalent (001) faces. The surface free energy of the (001) faces is nearly 1.4 times larger than that of the (101) faces. Therefore, the shape evolution in TiO_2 anatase was realized by modifying the surface free energy and growth rate of the nucleus with the surface adhesion of ligands. In addition, by controlling the cetyltrimethylammonium bromide and poly(ethylene oxide)$_{100}$–poly(propylene oxide)$_{65}$–poly(ethylene oxide)$_{100}$ as a surfactant and triblock co-polymer(F127), the NR shape and length were modulated. For the application of DSSCs, the TiO_2 NR film was sintered at a high temperature, while retaining the rod shape. This contributed to the achievement of a high conversion efficiency (7.29%) of light-to-electricity (J_{sc}: 13.1 mA/cm^2, V_{oc}: 0.767 V, fill factor: 0.728) with a thickness of 16 μm. This achievement was attributed to the increased rate of electron transport resulting from the high crystalline anatase NR and high dye loading.

2.2 Oriented Attachment Method

Oriented attachment involves the spontaneous self-organization of adjacent particles so that they share a common crystallographic orientation, followed by joining of these particles at a planar interface [20]. Bonding between the particles reduces the overall energy by removing the surface energy associated with unsatisfied bonds. Figure 3 shows how oriented attachment gives rise to

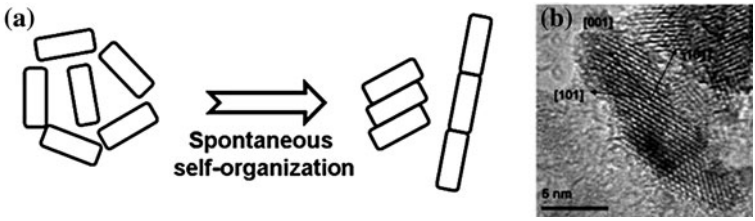

Fig. 3 **a** Simple schematic drawing of the oriented attachment mechanism, **b** TiO_2 nanorods synthesized by oriented attachment process

homogenous single crystals or to crystals separated by twin boundaries or other planar defects. This issue of morphological evolution is of direct importance to material science because growth and morphological evolution dramatically modify physical properties and surface reactivity.

Penn et al. reported the formation of anisotropic TiO_2 nanocrystals during hydrothermal treatment of TiO_2 nanocrystals under acidic conditions by oriented attachment [21]. Oriented attachment is important in nominally dry aggregates and in periodically wet environments. The particle movement needed to achieve orientation within random aggregates is provided by Brownian motion and other physical and energetic effects [22]. In addition, the researchers predicted that the particles are in contact with a solution under pH conditions near the isoelectric point. The organic molecules may hinder or modify oriented attachment by preventing contact between the faces on which adsorption has selectively occurred. Furthermore, they showed the evolution of the chains of particles, starting with the attachment of two primary crystallites. The attachment appears to occur most commonly on (112), less commonly on (001), and rarely on (101). This mechanism effectively serves to reduce the overall energy by eliminating the surfaces at which the crystallites join. In the most common case of (112) attachment, the highest surface energy face is eliminated.

Moreover, Hyeon et al. reported highly crystalline TiO_2 nanocrystals with various shapes and crystal structures in aqueous media at room temperature by oriented attachment [23]. In particular, the poly(ethylene glycol)-block-poly(propylene glycol)-block-poly(ethylene glycol) (PEO-PPO0-PEO) (P123) template controls the hydrolysis and condensation of the titanium tetraisopropoxide precursor. Under various reaction conditions, TiO_2 nanocrystals with different sizes and shapes were synthesized. With 1 M NaCl, spherical anatase nanocrystals with a particle size of 6 nm were produced, while in 1 M CH_3COOH solution, short anatase NRs with an average size of 4×20 nm were produced. Additionally, the addition of 1 M HCl induced the formation of long rutile NRs with an average size of 6×50 nm. These results reveal the essential presence of salt or acid to synthesize TiO_2 nanocrystals with unique shapes and crystal structures. In the DSSC, the photoanode comprised of oriented attachment. TiO_2 NRs showed the following two main advantages: (1) confirmation of high surface area directly proportional to the light-harvesting yield (dye uptake) resulted from the NRs synthesized from the necking of truncated NPs by recovering the low surface area of the general TiO_2 NRs, and (2) fast electron

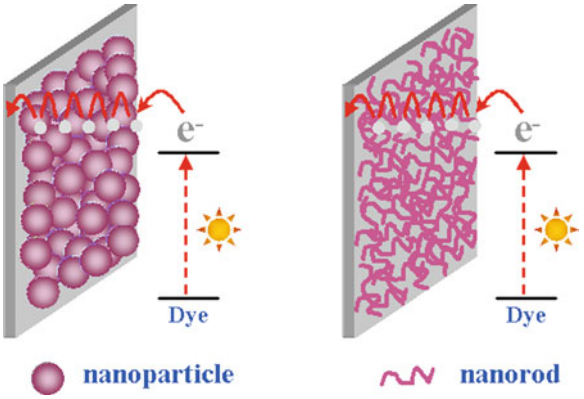

Scheme 1 TiO_2 photoanodes consisting of NPs and NRs in the configuration of DSSCs (Reprinted with permission from Ref. [24]. Copyright 2008 Wiley Interscience)

transport rate and degraded charge recombination from the decreased intercrystalline contacts between grain boundaries and specific directionality of NRs, bringing about the improved charge collection efficiency. To demonstrate the distinguished marks, the NP- and NR-based photoanodes for DSSCs were prepared in the same conditions (light-harvesting efficiency and charge injection yield). Only the charge transport ability of both samples was varied for comparison [24].

Scheme 1 describes the TiO_2 photoanodes consisting of the NPs and NRs in the configuration of DSSCs. At the same dye uptake ($n = 2.8 \times 10^{16}$), the deposited thickness variation between NP (5.47 μm) and NR (4.87 μm) films was small at approximately 10%. This indirectly indicates that NRs have a large surface area. From the photocurrent-voltage (J–V) measurements, a NP-based DSSC showed an V_{oc} of 0.68 V, a J_{sc} of 6.9 mA/cm^2, a FF of 0.71, and an efficiency (η) of 3.36%, while the NR-based DSSC exhibited results of 0.7 V, 11.7 mA/cm^2, 0.6, and 4.95%, respectively, under one sun condition.

To measure the electron transport and charge recombination characteristics between NP- and NR-based photoanodes in DSSCs, the stepped light-induced measurements of photocurrent and voltage (SLIM-PCV) was performed under front side illumination [25]. Then, truncated NRs with a particle size of about 6 nm were prepared as a control sample using the same synthesis tool.

Figure 4 shows the electron diffusion coefficients (D) and lifetimes (τ) of the NP-and NR-based DSSCs as a function of J_{sc}, as analyzed by SLIM-PCV. The D values of both samples showed a power-law dependence on the light intensity, indicating an aspect controlled by similar mechanistic factors [26]. The D value of the NR film was slightly higher than that of the NP film, showing that NR films have more favorable properties for electron transport than NP films. Considering the condition where small TiO_2 NPs (<10 nm) strongly bind to each other to decrease the unstable surface energy during thermal treatment, this minor improvement may be caused by the reduction of electron loss in the grain boundaries resulting from the necking of NPs, as well as by the increase of average crystallite size. From the parallel slope of both samples, similar traps were distributed over the whole range of the film because the slope indicates a steeper trap-state distribution. Figure 4b

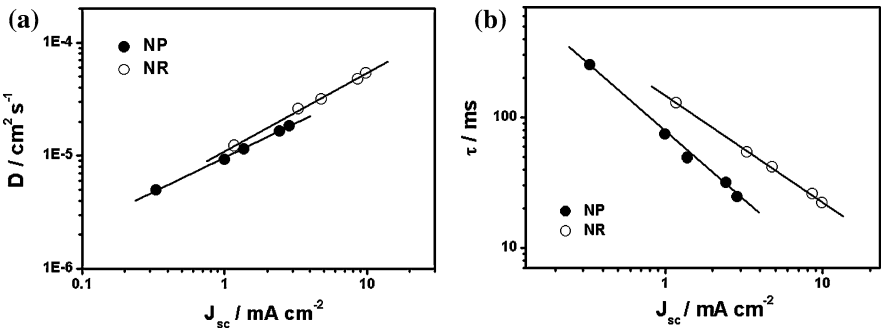

Fig. 4 Electron diffusion coefficients (D) and electron lifetimes (τ) for dye-sensitized NP and NR cells as a function J_{sc} controlled by ND filter from 635 nm laser illumination (Reprinted with permission from Ref. [24]. Copyright 2008 Wiley Interscience)

shows the values of τ as a function of J_{sc}. Over the light intensity range, the τ values of the NR films become an order of magnitude higher than those of the NP films. The lower lifetime of the NP films might be due to the combined effect of the downward band-edge shift, as confirmed by the relatively low V_{oc} value, and the increased charge recombination rate, as supported by dark current measurements (not shown here). This is mainly illustrated by the effects of the surface state, which leads to intraband gap states and enormous electron loss between the grain boundaries that experience tens of thousands of trapping/detrapping events during their transit through the film [27, 28]. The phenomenon indicates that more efficient DSSCs will be realized with a thicker TiO_2 NR layer than that in the NP film because both the enhanced electron transport due to the geometry effect and the increased electron lifetime due to the suppression of charge recombination contribute to increasing charge collection efficiency.

In a similar context, Adachi's group reported single-crystal-like TiO_2 NWs prepared by the oriented attachment mechanism using surfactant-assisted processes at a low temperature for highly efficient DSSCs [29]. The crystal growth direction of the oriented attachment was controlled by changing the molar ratio of acetylacetone to Ti, regulating the adsorption of surfactant molecules via control of the reaction rate and the surface energy. They showed that most of the aggregated particles form a wire shape with a single-crystalline (sc) structure. The oriented attachment occurred mainly in the (101) direction and formed a network structure. They suggested that the use of a (101) exposure plane with a network structure of single-crystal-like anatase NWs is one of the most promising methods because the intercrystalline titania contacts are greatly decreased by using a single-crystal-like network structure in comparison with a porous titania thin film composed of accumulated nanosized particle. This might be useful for easier electron transfer through the titania layer and suppression of back reaction of photoinjected electrons with I_3^-. This also influenced the 4-fold greater adsorption of ruthenium dye compared to P25. To summarize, a high light-to-electricity conversion rate of

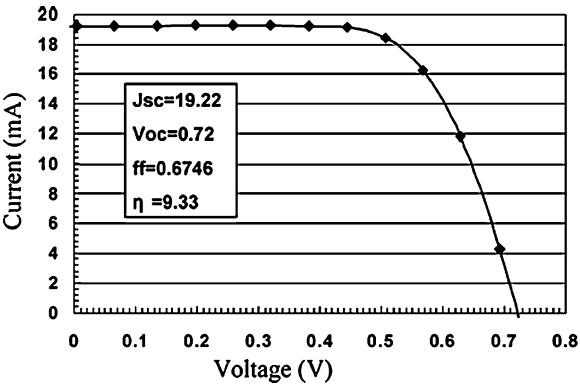

Fig. 5 Illustration of the photocurrent-voltage characteristics of the cell with titania thin film composed of a TiO_2 network structure of single-crystal-like anatase NWs (Reprinted with "Adapted" or "in part" permission from Ref. [29]. Copyright 2004 American Chemical Society)

9.33% (J_{sc}: 19.2 mA/cm^2, V_{oc}: 0.72 V, and FF: 0.675) was obtained for the cell with a TiO_2 network of single-crystalline anatase NWs (Fig. 5).

Furthermore, the hydrothermal process with the transparent TiO_2 sol prepared by peptization of anatase TiO_2 precipitates was suggested to dispersible and NR-like TiO_2 nanocrystals by an oriented attachment mechanism [30]. After further hydrothermal treatment of the mixture of NR-like TiO_2 nanocrystals and the original sol, branched and nanoring-like nanostructures with diameters of 6 nm in the anatase phase were obtained. When they were with the oriented crystallographic plane, more complex structures, such as nanoring-like and *T*-type TiO_2 nanostructures, were formed. By counting the number of the primary crystallites formed in the nanoring-like structures, about 20% of the nanocrystals were orientated and attached to the closed and nearly closed nanorings. They showed 2-fold higher ruthenium dye adsorption than commercial TiO_2 nanocrystals ST-01, giving a DSSC efficiency of 5.75%.

2.3 Sol–Gel Method

The sol–gel process is a wet-chemical technique regarded as a powerful approach for preparing dispersed NPs by tailoring the structure of a primary NP in which metal atoms are uniformly distributed. Such methods are initiated as soluble precursor molecules and are hydrolyzed to form a dispersion of colloidal particles (sol). As the reaction proceeds, the bonding of sol particles forms the integrated network of NPs (gel). The gel is typically heated to produce the desired materials. During this process, the metal alkoxides and metal chlorides as a precursor undergo various forms of hydrolysis and polycondensation reactions. To obtain homogenous macromolecular oxide networks for qualified nanomaterials in sol–gel processing, several factors in the reaction mixture (e.g., water, hydrolysis rate, precursor ratio etc.) must be controlled [31]. The key parameter to form 1-D TiO_2 NRs and NTs with the desired nanocrystalline structure and shape is the control of

the hydrolysis rate, due to the high reactivity of titanium precursors such as $TiCl_4$ and alkoxide [32]. In normal sol–gel processing, gelization and calcinations are necessary. If the calcination temperature for crystallization is not high enough, some organic molecules will remain in the product, leading to the incomplete crystallization of titania. On the other hand, if the temperature is too high, aggregation and phase transformation will occur, resulting in phase-impure product. Therefore, control over critical experimental parameters in the sol–gel reaction can lead to the formation of crystalline 1-D TiO_2 NR and NT.

Niihara et al. reported the synthesis of sol–gel derived TiO_2 NTs [33]. Needle-shaped TiO_2 crystals with diameters of 8 nm and lengths of 100 nm were obtained when sol–gel derived fine TiO_2-based powders were treated chemically with a 5–10 M NaOH aqueous solution for 20 h at 110°C, followed by the addition of HCl and distilled water in the solution. The following formation mechanism of titania NTs has been proposed: the crystalline raw material is first converted into an amorphous product through alkali treatment, after which the treatment with a distilled water and HCl aqueous solution results in the formation of titania NTs. This report is the first evidence that oxide NTs can be obtained easily via the sol–gel process without requiring molds for replication or templates.

Yanagida et al. reported the sol–gel synthesis of TiO_2 NTs with large aspect ratio and large specific surface area from P25 NP [34]. They optimized the fabrication conditions of DSSCs, i.e., the pH of the starting paste, sintering temperature for TiO_2 electrodes, electrolyte compositions, and $TiCl_4$ treatment, to give a conversion efficiency (7.1%) that was higher than that of the DSSC made of P25 (6.2%) due to the higher open-circuit voltage. To investigate comprehensively the high efficiency obtained by using the TiO_2 NT-based photoanode, the electron dynamic properties (electron diffusion coefficient (D) and lifetime (τ)) were examined (Fig. 6).

The D value of TiO_2 NTs was almost comparable with that of P25. The trend of diffusion coefficients was explained by the charge trap site density and distribution in the mesoporous electrode. The trap sites may have been formed mainly by grain boundaries and crystal defects. As for the grain boundaries, the number of boundaries across the TiO_2 film may not have decreased greatly because the orientation of NTs perpendicular to the conductive substrate had not been achieved in the TiO_2 NTs electrodes. On the other hand, the τ value in TiO_2 NTs electrode was about 3 times greater than that in P25, indicating that the probability of recombination between the electron in TiO_2 and the I_3^- in the electrolyte is smaller than that of P25. Considering both factors affecting the electron behavior, TiO_2 NTs were found to have longer diffusion length and thus more favorable electron transport property than P25.

More recently, the non-hydrolytic sol–gel method was successfully used for the synthesis of 1-D TiO_2 NRs by simultaneous modulation of the phase and size [35]. The synthesis of TiO_2 NRs was achieved with this reaction via the continuous delivery of two titanium precursors using two separate syringe pumps. By varying the injection rate of the precursors, the TiO_2 NRs simultaneously underwent phase transformation and length elongation. Furthermore, the morphology of the TiO_2 NRs evolved into a branched shape and their length was increased. In addition,

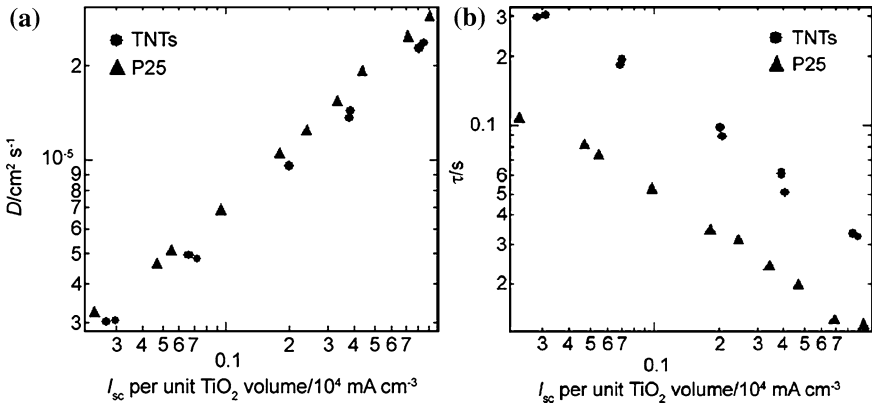

Fig. 6 Electron diffusion coefficients **a** and electron lifetimes **b** in the electrodes constructed with TiO_2 NTs (*circles*) and P25 (*triangles*) as a function of short-circuit photocurrent (I_{sc}) per unit TiO_2 volume (Ref. [34]-Reproduced by permission of the PCCP Owner Societies)

the crystalline phase of TiO_2 NRs was simultaneously affected by the injection rate. Pure anatase and pure rutile NRs were produced at fast and slow injection rates, respectively. Herein, the TiO_2 NRs were successfully employed as the photoanode for DSSCs. Particularly, the photoconversion efficiency (3.83%) of the mixture comprised of star-shaped rutile TiO_2 NRs and a small fraction of anatase NRs was comparable to that of P25 (4.1%).

2.4 Hydrothermal Method

Hydrothermal synthesis has been considered the most powerful technique to prepare single-crystalline 1-D TiO_2 nanomaterials that rely on the solubility of the precursor in hot water under high pressure. In particular, this method enables the growth of crystalline phases, which have unstable melting points, and materials showing high vapor pressure at their melting points can also be grown. Normally, the hydrothermal process is performed in an autoclave (steel pressure vessel) with Teflon® liners under controlled temperature and pressure. The hydrothermal process of TiO_2 nanomaterials under various experimental conditions (temperature, pH, and additives) yielded different morphologies and structural forms such as anatase, rutile, and even brookite. In general, the TiO_2 nanopowder is used as a precursor to form a suspension sol in the alkaline solution, and is subsequently hydrothermal treated to form TiO_2 NTs. On the other hand, alkaline titanate NTs were grown hydrothermally in alkaline solution, by exchanging the alkaline ions with protons to convert the alkaline titanate NTs to hydrogen titanate NTs. Afterward, TiO_2 NTs were produced by the thermal dehydration in air at high temperature or the hydrothermal reaction of hydrogen titanate NTs.

Initially, the production of uniformly nanosized rutile and anatase particles was carried out via the hydrothermal method [36]. Anatase and rutile phase TiO_2 were achieved by controlling the precursor ratio, hydrothermal conditions, and salt incorporation [37–39]. In addition, the hydrothermal synthesis of single-crystalline anatase TiO_2 NRs from NTs as the precursor in the absence of surfactants or templates was reported. In the strong basic solution (10 M NaOH), the pH of the NT suspension was controlled at different values by HNO_3 concentration. The crystal size of the anatase NPs obtained from the hydrothermal treatment increased with pH, and NRs with aspect ratios up to 6 and long axes along the anatase (001) were obtained at a pH slightly below 7. The mechanism of the tube-to-rod transformation was indicated by the local shrinkage of the tube walls to form anatase crystallites and the subsequent oriented attachment of crystallites to form NRs.

Subsequently, the hydrothermal synthesis (130°C for 72 h) of trititanate ($H_2Ti_3O_7$)-type NTs, with diameters of 9 nm and lengths of 100 to several hundreds of nanometers, using a single alkali treatment was suggested. In this method, TiO_2 reacts with a NaOH solution to form a highly disordered intermediate phase containing Ti, O, and Na [40, 41]. Single sheets of the trititanate $Ti_3O_7^{2-}$ started to grow inside the disordered phase. Afterward, when such trititanate sheets grew two-dimensionally, they simultaneously rolled up into NTs. When this reconstruction took place three-dimensionally, they suggested that $H_2Ti_3O_7$ plates with several trititanate layers were formed. The utilization of trititanate NTs with a multiwall structure as an electrode material in DSSCs was reported. These layered trititanate NTs showed highly efficient DSSC performance (7.5%: V_{oc} of 0.78 V, J_{sc} of 12.8 mA/cm^2, FF of 0.75) with a thickness of 14.4 μm. The incident photon to current efficiency (IPCE) at a wavelength of 520 nm was 61%. This indicated that the physicochemical characteristics of the trititanate NTs, including the high surface area, afforded a higher photocurrent density and a network structure useful for easier electron transfer through the titania layer, thereby suppressing the charge recombination between photoinjected electrons from the dye to the conduction band of the TiO_2 electrode and the I_3^- ions in the electrolyte.

Aydil et al. hydrothermally synthesized randomly oriented, anatase TiO_2 NWs on a titanium substrate using 10 M NaOH as an alkaline source [42]. During the hydrothermal reaction, the top surface of the titanium foil transformed to $Na_2Ti_2O_4(OH)_2$ NTs. Subsequently, the $Na_2Ti_2O_4(OH)_2$ NTs were converted by an ion exchange reaction to $Na_2Ti_2O_4(OH)_2$ NTs, which were in turn converted to polycrystalline anatase NWs through a topotactic transformation. The prepared TiO_2 NW film showed a photoconversion efficiency of about 1.8% (J_{sc}: 5.6 mA/cm^2, V_{oc}: 0.62 V, FF: 0.52). Additionally, IPCE as a function of wavelength typically reached 50% at 530 nm (the maximum absorbance of the dye). Furthermore, the researchers investigated the electron transport time constant using intensity modulated photocurrent/voltage spectroscopy (IMPS/VS) and photocurrent decay methods. Figure 7 shows the charge recombination and transport time constants for TiO_2 NW DSSCs as a function of J_{sc} (light intensity) [43].

The magnitude of the electron transport time (10^{-2}–10^{-3} s) and its dependence on the illumination intensity were similar to those reported for DSSCs made from

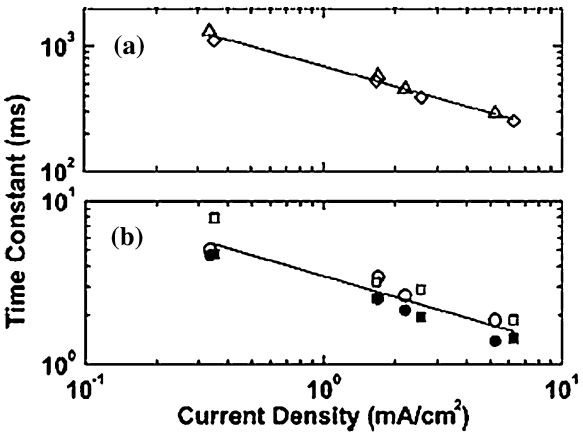

Fig. 7 **a** Charge recombination (Δ, ◇) and **b** transport (○, ●, □, ■) time constants for TiO_2 NW DSSCs as a function of J_{sc} (light intensity). In **b**, the open (○, □) and filled (●, ■) symbols represent transport times extracted from IMPS and photocurrent decay, respectively. Data for two cells (○, ●), and (□, ■) are shown to illustrate reproducibility. Similarly, recombination time constant data are shown for two different cells (◇, Δ) in **a** (Reprinted with permission from Ref. [43]. Copyright 2007, American Institute of Physics)

TiO_2 NPs, which exhibited a power-law dependence on J_{sc}. This indicated that the electron capture and release by surface traps determine transport times even in NWs, although the ratio of the electron recombination time to the electron collection time in NR solar cells was $\sim$150, larger than that observed in the NP DSSCs, resulting in an electron collection efficiency of nearly 100%. They presented two reasons for the longer recombination times observed in NWs relative to NPs. First, the diameter of the TiO_2 NWs is larger than both the diameter of typical TiO_2 NRs used for assembling DSSCs and the semiconductor's Debye length. This larger diameter and the cylindrical geometry allow the wires to support radial electric fields that keep the electrons away from the NW surface, thereby reducing surface electron densities and recombination. A second possibility is that the NWs and NPs have different spatial distributions of electron traps. In nanowire, a fraction of the traps may be at the internal grain boundaries, not exposed to the electrolyte.

Utilizing the TiO_2 NRs, several approaches to increase the specific surface area, and thereby improve the photoconversion efficiency, were tried by several researchers [44–46]. At first, the DSSC photoanode was composed of a composite of anatase TiO_2 NPs and single-crystalline anatase TiO_2 NWs [44]. The composite electrode showed a high surface area from NP aggregates and the fast electron transport rate and light scattering effect of NWs. At the optimum content (20 wt%) of TiO_2 NWs, the conversion efficiency ($\eta = 8.6\%$) was improved more than that ($\eta = 6.7\%$) of pure NP cells. In addition, they indirectly showed that the improved electron diffusion length of the composite electrode was caused by the continuous increase in the current density with increasing film thickness over the whole thickness range up to 17 μm. In addition, in the situation where the TiO_2 NWs baked

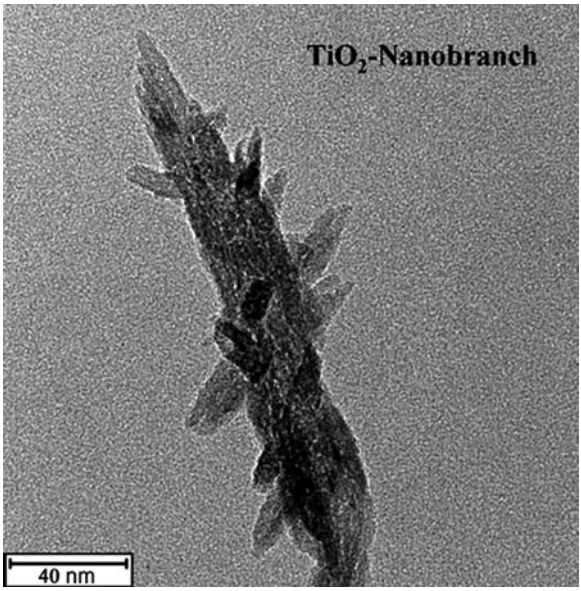

Fig. 8 FE-TEM image of the TiO_2 nanobranched structure (Reprinted with permission from Ref. [46]. Copyright 2010 American Chemical Society)

at 450–500°C showed a significant morphology change to NP, the niobium treatment of TiO_2 NWs acted to decrease the Na^+ content effectively and increase the thermal stability of NWs [45]. DSSCs composed of a mixture of TiO_2 NPs (P25) and the niobium-treated NWs (1:1 wt%) showed a photoconversion efficiency of 5.15% (V_{oc}: 0.78 V, J_{sc}: 11.2 mA/cm^2, FF: 0.59) compared to 4.73% (V_{oc} of 0.73, J_{sc}: 9.52 mA/cm2, FF: 0.68) of P25-based DSSCs. In addition, the branched TiO_2 NPs were synthesized by seeding with TiO_2 NWs, thereby transforming from NWs to a nanobranched shape [46]. Figure 8 shows the field-emission transmission electron microscopy (FE-TEM) image of the synthesized nanobranched structure.

Relative to a typical TiO_2 NW with few dye adsorption sites, the nanobranched TiO_2 showed the high roughness factor up to two times and thus the enhancement of charge harvesting efficiency. In the fabrication process of TiO_2 film, the high-temperature annealing did not affect the morphological modification of nanobranched TiO_2, so that the photocurrent and cell efficiency were enhanced from 6.25 mA/cm^2 (TiO_2 NW) to 12.18 mA/cm^2 (nanobranched TiO_2) and from 2.6 to 4.3%, respectively.

3 Preparation of Self-Ordered TiO_2 Nanorod/Nanotube Films for Dye-Sensitized Solar Cells

1-D TiO_2 NRs or NTs synthesized by chemical approach showed a randomly oriented, nanostructured electrode after the thin film formation for DSSCs. This randomly mixed film caused the degradation of the originally unique properties

in the electron transport, similar to in the NP system [43]. The structural disorder at the contact between two crystalline NRs or NTs leads to enhanced scattering of free electrons, thus reducing electron mobility. Accordingly, to benefit from the improved electron transport in elongated nanostructures, it is necessary to assemble nanostructures directly on the surface of the electrode. More recently, ordered and strongly interconnected TiO_2 NTs on the Ti substrate has attracted attention as a fascinating material that offers a large internal surface area without damaging the geometrical and structural order. The precisely oriented nature of TiO_2 NT arrays makes them excellent electron percolation pathways for vertical charge transfer between the interfaces. Furthermore, TiO_2 NTs arrays show outstanding charge transport and carrier lifetime properties, and have been found to be suitable for a variety of applications, including Li-ion batteries, photoelectrolysis, and DSSCs [47, 48]. Furthermore, arrays of single-crystalline TiO_2 NWs on Ti foil were prepared by a novel alkali hydrothermal growth process. DSSCs using TiO_2 NWs arrays are promising prospects in research in this field. To minimize the light loss from back-side illumination, the TiO_2 NWs were prepared on an FTO substrate under hydrothermal conditions. This research is closely correlated with application to various types of solar cells, including DSSCs, heterojunction, hybrid, and organic solar cells [49–51]. The control of diverse experimental conditions such as film growth time, substrate, initial reaction concentration, acidity, titanium precursor, and surfactants or salts was reported for the DSSCs. As another synthesis tool, large oriented arrays and continuous films of TiO_2-based NTs were prepared by hydrothermal process on the Ti substrate. Several methodologies (electrochemical anodization and hydrothermal reactions) to form self-ordered TiO_2 NRs/NTs on the substrate are summarized in detail below.

3.1 Electrochemical Anodization of TiO_2 NTs on Ti for DSSCs

3.1.1 Electrochemical Anodization in Aqueous Electrolyte

In 1999, Zwilling et al. first reported titania films with porous surfaces formed by anodizing Ti metal in an F^- ion-based electrolyte [52]. Approximately 300 nm-thick TiO_2 NTs were formed on the Ti foil. The thin TiO_2 NTs were restricted to applications to other fields. Afterward, the tubular shape and length were optimized in the F^- ion-based electrolyte by tuning the pH, electrolyte concentration, and precursor species [53–55]. Schmuki et al. reported the fabrication of a 2.5 μm-thick TiO_2 NT array using NH_4F as a fluorine source [53] and Grimes et al. also succeeded in forming a longer TiO_2 NT (up to 4.4 μm) array using KF and NaF instead of HF as a precursor [54]. The key to achieve high-aspect-ratio growth is adjustment of the dissolution rate of TiO_2 by localized acidification at the pore bottom while a protective environment is maintained

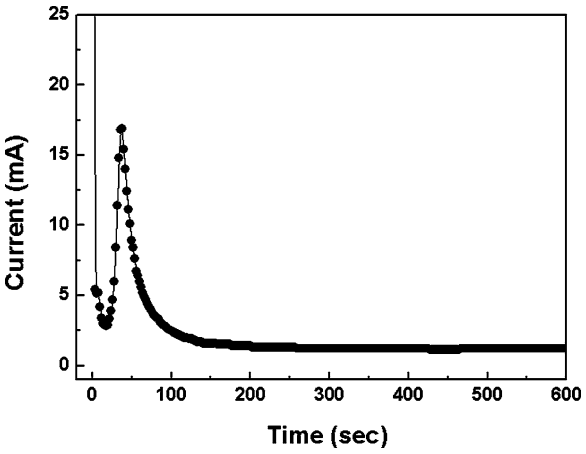

Fig. 9 Current-time response at a constant voltage of 20 V at pH 4.2 electrolyte using NaF precursor

along the pore walls and at the pore mouth [55]. Figure 9 shows the current density as a function of the anodization time in 10 min intervals.

In the initial stage of anodization (up to 30 s), an abrupt decrease of the current related to the formation of a barrier layer was followed by a sudden increase of current due to the active chemical dissolution reaction of the oxide layer formed by F^- ions from the electrolyte, leading to the formation of a porous structure. In the final stage, a relatively constant equilibrium state was maintained with increasing anodization time, while the current density slightly increased, showing an oscillation curve. In the equilibrium condition between the electrochemical formation of TiO_2 at the pore bottom and the chemical dissolution of this TiO_2 layer in the F^- ion-containing electrolyte, the TiO_2 NTs were grown continuously. The related mechanistic process for the formation of self-ordered titanium dioxide has been reported [56].

$$Ti^{4+} + 2H_2O \rightarrow TiO_2 + 4H^+ (\text{Hydrolysis of Ti}) \quad (1)$$

$$TiO_2 + 6HF \rightarrow [TiF_6]^{2-} + 2H_2O + 2H^+ (\text{Dissolution of } TiO_2) \quad (2)$$

The above reactions proceed alternatively in the overall reaction. Because the key to achieve longer TiO_2 NTs is control of the dissolution rate of TiO_2, which is highly dependent on the pH value, for the growth of high-aspect-ratio TiO_2 NTs. Figure 10 shows the field emission scanning electron microscope (FE-SEM), top- and cross-sectional views of TiO_2 NTs for various electrolyte pH values adjusted by a NaOH reagent.

The length of the TiO_2 NTs is dependent on the electrolyte's pH [57]. The length of the nanotubular layer gradually increases with increasing pH, being 1, 1.3, 1.7, and 2.6 μm at pH 1.5, 2.3, 3.6, and 4.2, respectively. In a strongly acidic electrolyte, there are enough H^+ ions to increase the chemical dissolution rate of the thin titanium dioxide layer formed on the pore bottom. If the chemical dissolution reaction is dominant, it limits the growth of the nanotubular TiO_2 layer

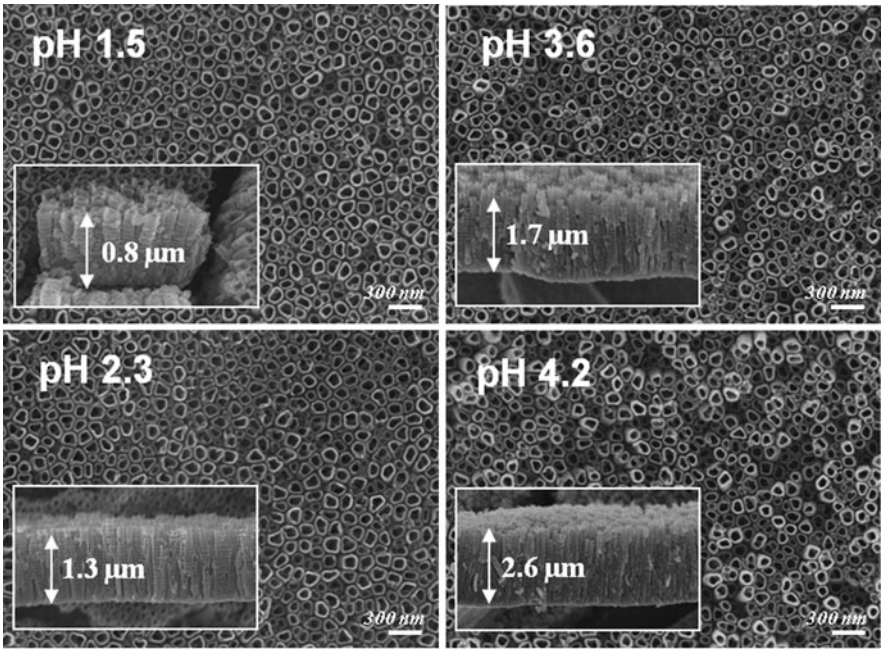

Fig. 10 FE-SEM top- and cross-sectional views of TiO_2 NTs for various electrolyte pH values adjusted by a NaOH reagent: **a** pH 1.5, **b** pH 2.3, **c** pH 3.6, and **d** pH 4.2

because the anodic electrolyte-containing F^- ions is directly connected to the bare Ti substrate, instead of the titanium dioxide layer, which terminates the anodic reaction. On the other hand, in a weakly acidic electrolyte, the chemical dissolution rate is retarded because the quantity of H^+ ions is decreased by Eq. 2, and is accompanied by a slight increase in the rate of the chemical oxidation reaction so that thicker anodic TiO_2 NTs are formed. In this condition, thicker TiO_2 NTs were grown. Above pH 5, thick TiO_2 layers with densely connected NPs were grown, instead of self-ordered TiO_2 NTs. In this case, the surface morphology exhibits a dendrite structure, which is formed due to the limited ion concentrations (not shown here). These are influenced by the limited ion concentration of the electrolyte and duration of anodization. The reduced number of H^+ ions at the pore bottom degrades the chemical dissolution rate and causes the formation of a thick and compact TiO_2 layer with dendrite-shaped surface morphology. All of the grown TiO_2 NTs were interconnected with a constant strain maintained among them to impede the formation of the exceptionally dominant grown TiO_2 NT that leans in the downward direction and limits the thickness of TiO_2 NTs.

Employing the TiO_2 NTs as a photoanode, the DSSCs were fabricated under the back-side illumination condition. Scheme 2 shows a representative diagram of a back-side illumination, NT-array dye solar cell [58]. Approximately 6 µm-thick TiO_2 NTs, grown in an electrolyte composed of 0.1 M KF, 1 M $NaHSO_4$, and 0.2 M

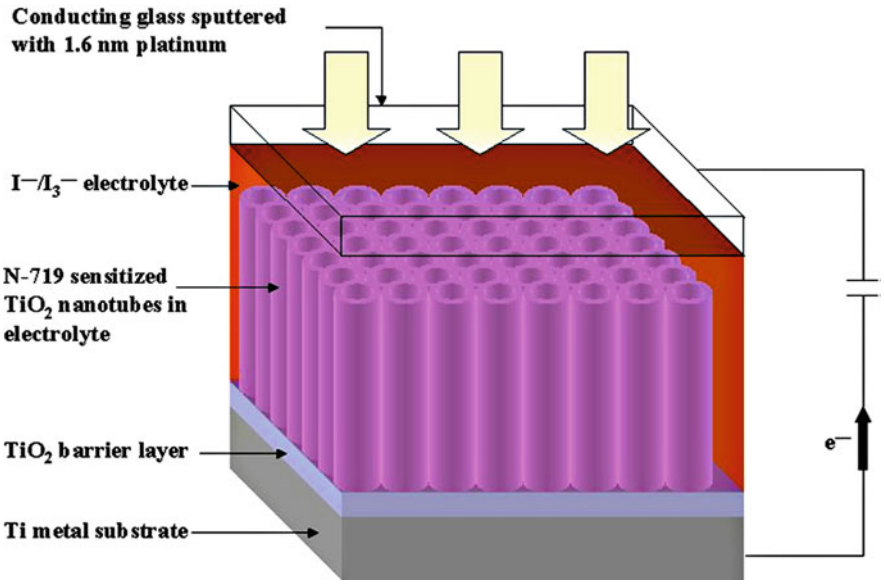

Scheme 2 Simple diagram describing a back-side illumination nanotube array dye-sensitized solar cell (Reprinted with permission from Ref. [58]. Copyright 2006 IOP Publishing Ltd.)

trisodium citrate with NaOH added to adjust the pH 5.0, were applied to the DSSCs with a resultant conversion efficiency of 4.24% (V_{oc}: 0.84 V, J_{sc}: 8.79 mA/cm^2, FF: 0.57) in the N719 dye dissolved in acetonitrile solvent. By adjusting the anodization conditions, such as the electrolyte composition and the anodization methods, different TiO_2 NTs with thicknesses of 1–2.5 μm (potential-sweeping) and 30 μm (rapid breakdown) were fabricated for the DSSCs [59]. The conversion efficiency was about 0.05% with 1–2.5 μm-thick TiO_2 NTs and 0.54% with 30 μm-thick TiO_2 NTs under back-side illumination. In addition, solid-state DSSCs with TiO_2 NTs electrodes were also made to use the easy penetration of viscous electrolyte along the large inner pores. At first, straight-stranded anatase TiO_2 NTs were produced by anodic oxidation on a pure titanium substrate in an aqueous solution containing a 0.45 wt% NaF electrolyte at a fixed pH of 4.3 [60]. The average length of the TiO_2 NTs was approximately 3 μm. To improve the conversion efficiency by retarding the charge recombination between the TiO_2 NT film and redox electrolyte, a thin ZnO shell was coated on the TiO_2 NT film, which increased V_{oc} (0.64–0.71 V) and J_{sc} (2.38–2.68 mA/cm^2), but similar FF (38–37%). Scheme 3 shows the interfacial charge-transfer process at the ZnO-coated TiO_2/dye/electrolyte of DSSC. To increase the FF, chemical etching was performed using hydrogen peroxide to reduce the compact TiO_2 layer formed between TiO_2 NT and the Ti foil, giving a final conversion efficiency of 0.906% (V_{oc}: 0.693 V, J_{sc}: 2.67 mA/cm^2, FF: 49%) with ZnO coating and chemical etching effect, compared to 0.578% for bare TiO_2 NT-based solid-state DSSCs.

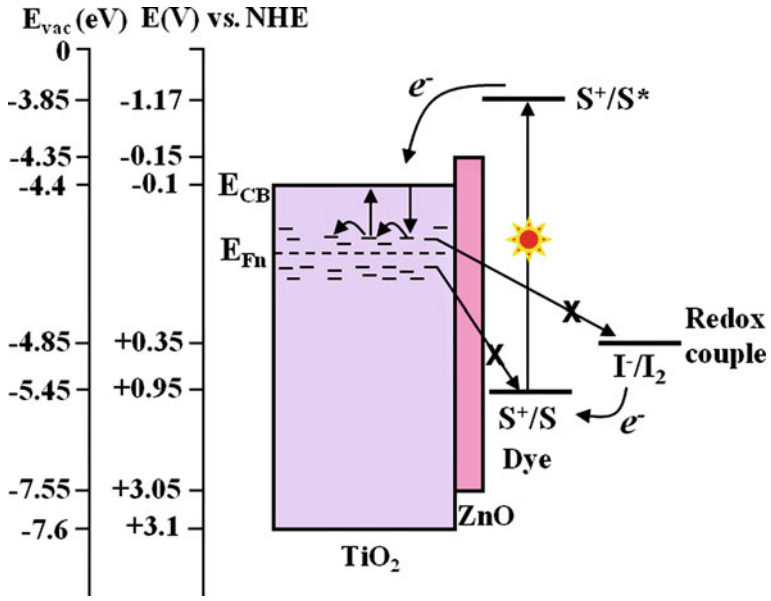

Scheme 3 Interfacial charge-transfer process at the ZnO-coated TiO_2/dye/electrolyte of DSSCs. Trapping/detrapping events of photoinjected electrons between the conduction band and trap sites of TiO_2 are shown in the region of E_{Fn} (Reprinted with permission from Ref. [60]. Copyright 2007 American Chemical Society)

Following from this result, the influence of ZnO coating in the charge-transfer process on the term of electron lifetime was investigated using open-circuit voltage decay (OCVD) [61]. Figure 11 shows the OCVD result from bare and ZnO-coated TiO_2 NTs. After 10 s of illumination, exponential decay of the photovoltage occurred immediately, followed by a steady decease. The ZnO-coated sample showed no significant change, while the bare TiO_2 film showed an irregular curve in the low photovoltage region. From the decay curve of the photo-voltage, the electron lifetime was calculated by applying Eq. 3, where k_BT is thermal energy, e is the electronic charge, and dV_{oc}/dt is the derivative of the open-circuit voltage transient.

$$\tau = -\frac{k_B T}{e}\left(\frac{dV_{oc}}{dt}\right)^{-1} \tag{3}$$

From this result, the ZnO-coated TiO_2 film showed a longer electron lifetime in the scanned potential range, indicating that more electrons were survived from the back-reaction, improving the photocurrent. On the other hand, the linear curve of the bare TiO_2 NT arrays showed some deviation in the low potential region, from 0.25 to 0.35 V, indicative of the formation of interfacial charge transfer from the trap/surface states to the cations of the redox electrolyte [62].

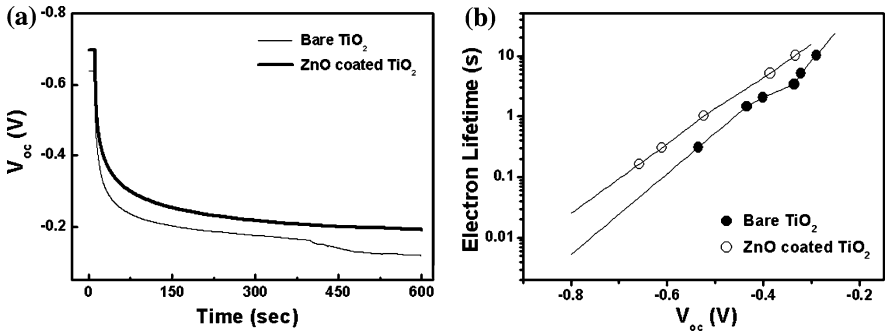

Fig. 11 The curves of the open-circuit voltage decay (OCVD) of the bare and ZnO-coated TiO_2 NTs: **a** the profile of the V_{oc} decay as a function of time, and **b** the log-plot of the electron lifetime as a function of V_{oc} (Reprinted with permission from Ref. [60]. Copyright 2007 American Chemical Society)

3.1.2 Electrochemical Anodization in the Organic Electrolyte

In the next step, the research focused on the growth of longer TiO_2 NT arrays in a polar organic-based electrolyte containing F^- ions. In the aqueous electrolyte, the thickness of the growing TiO_2 NTs was limited by a fast chemical dissolution process with the F^- ions and the concurrent chemical etching process on the top region of the tubular structure. In addition, the walls showed considerable disorder, like sidewall ripples and other etch effects. However, in the organic media containing the fluoride source, very long TiO_2 NTs with significantly improved tube wall roughness (smooth and high-aspect-ratio NTs) were formed on the Ti foil by controlling the high power potential and solvent species [63, 64]. In general, the anodization process occurred simultaneously in the three processes and was governed by (1) the field-assisted oxidation of Ti metal to form TiO_2, (2) the field-assisted dissolution of Ti metal ions in the electrolyte, and (3) the chemical dissolution of Ti and TiO_2 due to chemical etching by F^- ions [65].

Figure 12 shows the current transient as a function of anodization time in the ethylene glycol-based electrolyte containing 0.25 wt% NH_4F and 2 wt% water. In the initial stage (<100 s), gas evolution dominated from electronic conduction, which was attributed to the formation of a thinner oxide layer in the organic electrolyte. This is indicative of electronic conduction's dominance in the early part of the process. The current drops steeply thereafter due to the initial formation of an insulating oxide layer. In this region, electronic conduction decreases due to the blocking effect of the formed oxide layer and ionic conduction through the TiO_2 increases. Once the oxide layer is completely formed over the entire exposed surface of the anode, electronic conduction through the TiO_2 barrier layer becomes negligible and ionic conduction dominates the mechanistic behavior. The thinner oxide layer allows much greater ionic conduction than in aqueous electrolytes and faster movement of the Ti/TiO_2 interface into the Ti substrate, ultimately enabling substantial increases in NT length. Moreover, the higher anodization potential

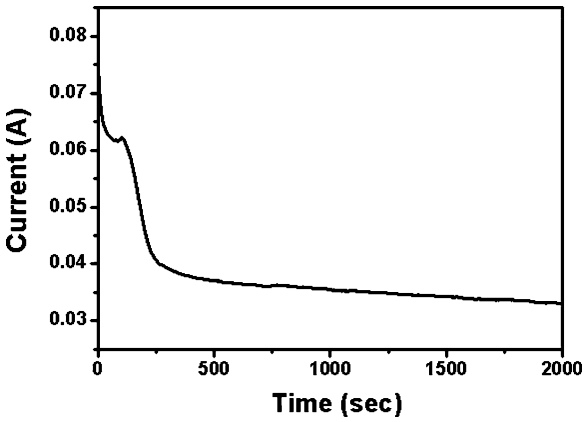

Fig. 12 Current-voltage profile during the anodization process in the organic electrolyte

exerts a greater driving force for both electronic and ionic conduction. As the anodization proceeds and the real surface area available for anodization is reduced, the current density is decreased in the final state.

Figure 13 displays the FE-SEM images of 10 μm-long TiO_2 NTs grown in ethylene–glycol-based electrolyte for 1 h anodization. Compared to TiO_2 NTs grown in aqueous electrolyte, well-aligned TiO_2 NTs with smooth wall were produced [66]. Depending on the anodization time, the length was controlled by a linear dependence. Furthermore, self-standing, 720 μm-thick TiO_2 NTs were fabricated using a double-sided electrochemical oxidation of Ti in an electrolyte comprised of water, NH_4F, and ethylene glycol [67]. From the effects of electrolyte composition, applied potential, and anodization duration on the length and diameter of the NTs, it was suggested that the reduced hydroxyl ion injected from the electrolyte, which enables faster high-field ionic conduction through the barrier layer, is responsible for the high NT growth rates.

Frank et al. studied the microstructure and dynamics of electron transport and recombination in DSSCs incorporating oriented TiO_2 NT arrays with a TiO_2 NP film as a control sample [68]. The arrays consisted of closely packed NTs several micrometers in length according to the anodization time, with typical wall thicknesses and intertube spacings of 8–10 nm and pore diameters of about 30 nm. The calcined material was fully crystalline with individual NTs consisting of approximately 30 nm-diameter crystallites. The transport and recombination properties of the NT and NP films used in DSSCs exhibited comparable transport times, while recombination was much slower in the NT films, indicating that the NT-based DSSCs have significantly higher charge-collection efficiencies (25%) than the NP-based films (Fig. 14).

This indicates that NT films can be made thicker than NP films for a given recombination loss. Besides, NT films exhibit higher light-harvesting efficiencies because of their stronger light-scattering effects. Accordingly, the conversion efficiencies of NT-based DSSCs were comparable or superior to those of NP film-based DSSCs of the same thickness.

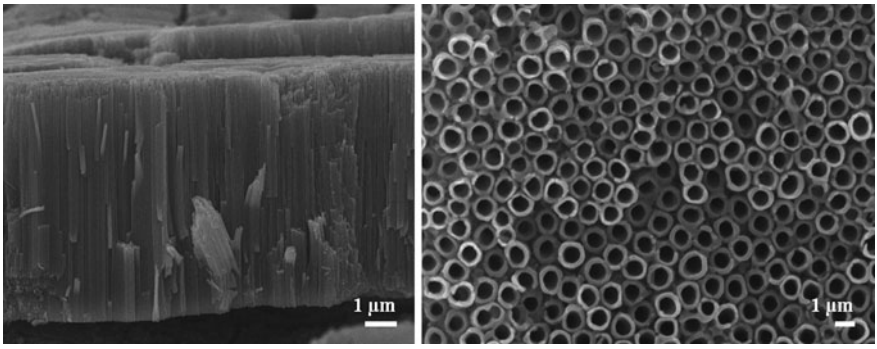

Fig. 13 FE-SEM images of TiO_2 NT arrays grown in ethylene–glycol-based electrolyte (Reprinted from Ref. [66]. Copyright 2008 with permission from Elsevier)

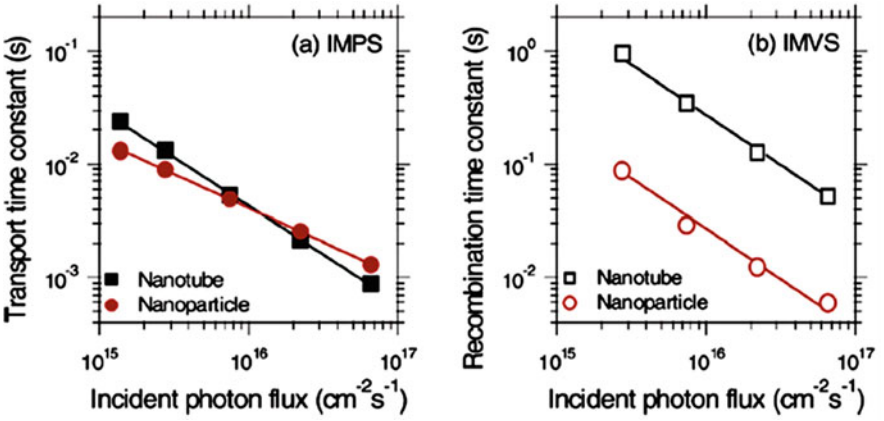

Fig. 14 Electron transport properties of TiO_2 NP and NT based DSSCs (Reprinted with permission from Ref. [68]. Copyright 2007 American Chemical Society)

However, with increasing anodization duration, the surface morphology became rough after an ultrasonic cleaning. Since the rough surface morphology affects light absorption and scattering under the illumination, uniform and self-ordered TiO_2 NTs, which look like anodic aluminum oxide, were formed by pretreatment of the Ti substrate [69]. Figure 15 shows the pretreated Ti substrate and the surface morphology after two-step anodization process. The TiO_2 NTs grown by two-step anodization showed a uniform surface morphology and thinner walls with a united wall structure between the pores like an aluminum oxide membrane, while one-step TiO_2 NTs showed a separated wall structure. The dependence of the electron behavior on the surface morphology of TiO_2 NTs in the DSSC was investigated. Anodically grown TiO_2 NTs, approximately 13 μm thick, were prepared on an ethylene glycol-based electrolyte. The TiO_2 NTs grown on the pretreated substrate showed uniform surface morphology with an

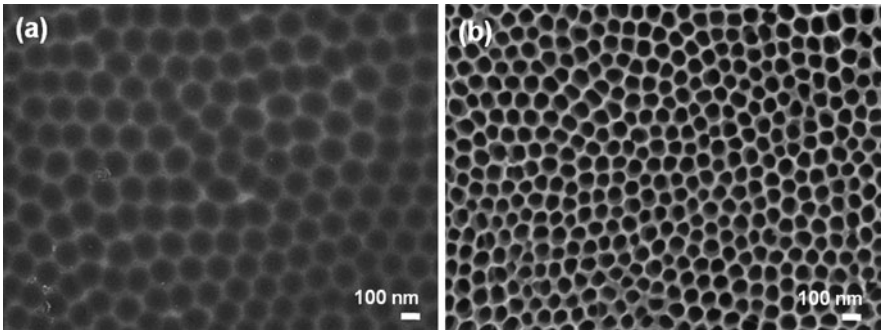

Fig. 15 FE-SEM images of pretreated Ti substrate and TiO_2 nanotube grown on pretreated Ti substrate (Reprinted with permission from Ref. [69]. Copyright 2009 IOP Publishing Ltd.)

interconnected nanotubular structure, while the surface morphology of the TiO_2 NTs formed on the bare substrate was quite rough. The photocurrent (8.4 mA/cm^2) of two-step TiO_2 NT-based DSSC was improved by 14% compared to that (7.2 mA/cm^2) of one-step TiO_2 NT-based DSSC. This improvement was attributed mainly to the increased light-harvesting efficiency (21%), that is, the light absorbance by a dye-sensitized TiO_2 NT film.

This was confirmed by a dye desorption experiment in NaOH after dye uptake. The discrepancy between the increasing light-harvesting yield (21%) and the overall photocurrent (14%) was attributed to the slow electron transport rate, a result of the large surface area and lateral movement along the 3-D network. Figure 16 shows the electron diffusion coefficient (D) and lifetimes in the DSSCs based on the one- and two-step TiO_2 NT electrodes with thicknesses of 7.5 $\pm$ 2.84 μm. The D values of the one-step TiO_2 NT-based DSSC were higher than those of the two-step TiO_2 NT-based DSSC over the light intensity range because the electrons in the two-step TiO_2 NT electrode were transported through a 3-D network instead of a 1-D conducting path. Generally, charge transport along a 3-D conducting path is slower than that along a 1-D conducting path because lateral movement reduces the transport rate significantly. The second explanation is that traps are located on or near the surface of the TiO_2 NPs, which are known as near-surface states. These reduce the electron transport rate with increasing internal surface area, which increases the number of traps sites. The mean surface area of the two-step TONT film was 21% higher than that of the one-step TiO_2 NT film. A third possible cause for inhibited electron diffusion is the wall thickness (electron pathway). The two-step TiO_2 had thinner walls and the jointed wall structure between the inner pores, while the pores of one-step TiO_2 NTs were divided separately. This means that the wall structure of the two-step TiO_2 NTs is unfavorable for electron transport.

On the other hand, the τ of the one-step TiO_2 NTs was lower than that of the two-step TiO_2 NT, possibly because of the distribution of traps near the surface region. In the case of the one-step TiO_2 NTs, the separation of each NT changes

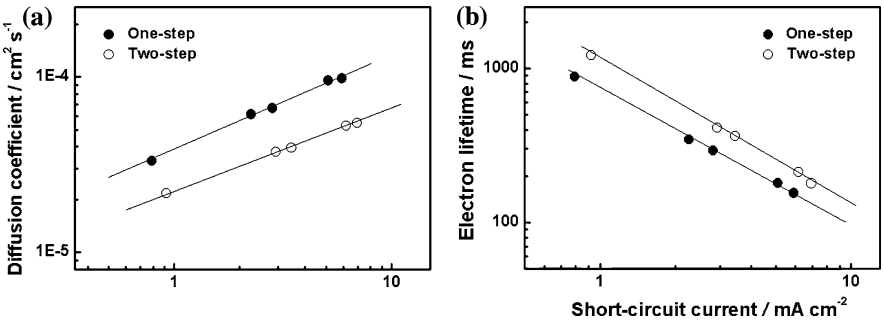

Fig. 16 **a** D and **b** τ in the DSSCs based on the one- and two-step, TONT electrode with a thickness of 7.5 ± 2.84 μm (Reprinted with permission from Ref. [69]. Copyright 2009 IOP Publishing Ltd.)

the transport mechanism to a mixture of one and three dimensions because each NT is bound strongly. The decrease in internal surface area is closely related to the decrease in trap site density. Photoinjected electrons were trapped preferentially on the energetically stable trap sites below the Fermi level. Electron transport to the contact involves multiple trapping events, which were modeled as the trapping and detrapping (thermal release) of the electrons along the distributed trap states. Unstable electrons in the conduction band leave after occupying the limited trap sites and can react easily with the cations from the redox electrolyte to maintain an energetically stable state. This might reduce the electron lifetimes on the one-step TiO_2 NT. Although the L value of two-step TiO_2 NT-based DSSCs is lower than that of one-step TiO_2 NT-based DSSCs, the L value is considerably higher than that of the NP-based DSSCs, suggesting that the nanotubular structure can support a thicker TiO_2 film for more efficient DSSCs. Therefore, the improved photocurrent of the two-step TiO_2 NT-based DSSC led to an enhancement (12.5%) of the overall power conversion efficiency.

Moreover, the diverse experimental conditions for electrochemical anodization affect the geometry and surface properties of the NT arrays [70–73]. Using appropriate alternating voltage switches between conditions, enabling tube growth and leading to a compact layer named the bamboo type structure [70]. By using different alternating voltage pulse durations, the distance between the bamboo rings can be adjusted. This structure resulted in an improved conversion efficiency of DSSCs due to the higher dye loading per unit volume by the bamboo ring, compared to normal NT structure where the carrier transport and recombination kinetics of bamboo and normal NT structure showed similar trends. The top surface morphology of the TONT was adjusted by several methods because this region is closely associated with electron transport and electrolyte penetration in DSSCs. To prevent the bundling and microcracks of oriented, NT film arrays, the supercritical CO_2 drying technique and the deposition of blocking layer composed of rutile-type oxide layers were widely used to grow the uniform self-ordered TiO_2 NT film [71]. Based on basic research on the TiO_2 NTs, the improvement of the photoconversion

efficiency of the TiO_2 NT-based DSSC was also attractive because its maximum is about 4%. The main disadvantage of the TiO_2 NT electrode in DSSCs is the low surface area, especially in the case of TiO_2 NTs composed of large pores (>100 nm). Therefore, a $TiCl_4$ treatment of all areas of TiO_2 NTs was used to increase the dye adsorption area. Recently, the DSSC efficiency was doubled from 1.9 to 3.8% by such a treatment [72]. Then, 3 nm-sized TiO_2 nanocrystallites were uniformly coated on the surface region and annealed afterward. The amorphous TiO_2 NTs were transformed to anatase TiO_2 NTs by annealing at about 350°C, followed by the $TiCl_4$ treatment and, finally, annealing again at 450°C for 30 min. This research showed the potential for TiO_2 NT-based DSSCs to achieve a high efficiency. In addition, MgO was "coated" on the TiO_2 NT surface as an energy barrier to increase the efficiency by an order of magnitude higher than that of the MgO using bare TiO_2 NTs [73]. This was elucidated by the reduction of charge recombination between the TiO_2 and electrolyte and the improvement of dye adsorption due to the basicity of the MgO surface.

3.1.3 Electrochemical Anodization of Sputtered Grown Ti Metal on TCO Substrate for DSSCs

The micron-length TiO_2 NTs grown on opaque Ti foil should utilize back-side illumination from the counter electrode side to measure the DSSC efficiency. This structure decreases the total absorbing visible light because the light must pass through the counter-electrode and the light-absorbing electrolyte. Approximately 25% of the incident solar energy that is lost from the counter side can be recovered from the Ti metal film on the TCO substrate [74]. Grimes et al. reported highly ordered transparent TiO_2 NT arrays on TCO substrates in DSSCs [75]. The critical point to form transparent TiO_2 NTs on the FTO is the fabrication of a high quality Ti thin film grown at a high substrate temperature (500°C) and a slow sputtering rate during the sputtering process. After the electrochemical anodization at a constant potential of 12 V in an electrolyte of 0.5% HF and acetic acid mixed in a 7:1 ratio (constant temperature: 5°C), highly ordered NT arrays of 46 nm pore diameter, 17 nm wall thickness, and 360 nm length were grown perpendicular to a FTO-coated glass substrate. The $TiCl_4$ treatment on TiO_2 NTs enhanced the photocurrent in the commercial DSSC structure using ruthenium-based dyes. A photocurrent efficiency of 2.9% was attained with 360 nm-thick TiO_2 NTs. Furthermore, it was revealed that the highly ordered TiO_2 NT arrays, in comparison to nanoparticulate systems, have superior electron lifetimes and provide excellent pathways for electron percolation from voltage-decay measurements (Fig. 17). Furthermore, they succeeded in growing the highly ordered TiO_2 NTs (above 30 μm) on the FTO substrate 3 years later [76]. By employing several advantages of the TiO_2 NT structure, enhanced charge harvesting in the near-infrared region of the solar spectrum was thereby enabled. Three challenges remain to be overcome in the fabrication of transparent TiO_2 NT array films with extended lengths. The first is the formation

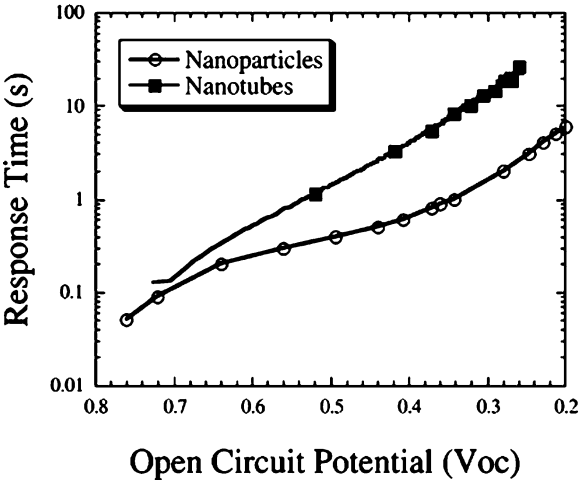

Fig. 17 Response time according to V_{oc} decay for a transparent TiO_2 NT array DSSC as well as the response time for a TiO_2 NP DSSC (Reprinted with permission from Ref. [75]. Copyright 2006 American Chemical Society)

of uniform, nonporous TiO_2 films with thicknesses of tens of micrometers and sufficient adhesion to the FTO glass layer. Second, the anodization of these thick TiO_2 films until uniform optical transparency is achieved. Finally, the third is the absence of any debris or clumping of the very long NTs after the anodization in the fluorine-containing, non-aqueous organic electrolytes. These challenges were overcome by the growth of a high quality Ti metal film on a FTO substrate and an appropriate electrolyte conductivity was selected to minimize interface etching and the surface debris problem, thus yielding long, uniform, non-clumped,and debris-free transparent NT array films. DSSCs were then fabricated using these TiO_2 NTs. Depending on the TiO_2 NT thickness, the efficiency ranged from 2.57% (1.2 μm) to 6.86% (20 μm). Even though the TiO_2 NT thickness was increased up to 33 μm, the efficiency remained low relative to that of NP DSSCs (10–11%). The major limitation of the power efficiency of NT DSSCs is their low FFs, which are about 25% lower than those of NP DSSCs. This was attributed to the degradation of the FTO film occurring during the extended, high-temperature treatment of the NTs for improving crystallinity and oxidizing trace metals under the NT film. It is expected that more efficient DSSCs will be fabricated after these problems are eliminated.

3.2 Hydrothermal Reaction for Growing TiO_2 NWs/NTs on Ti and TCO Substrates for DSSCS

Recently, several fascinating results related to TiO_2 NWs directly grown on the substrate were produced by hydrothermal process. The first is the growth of oriented, single-crystalline TiO_2 NW arrays on Ti foil [77]. After the formation of single

crystal, sodium titanate NWs ($Na_2Ti_2O_5{\cdot}H_2O$), protonated bititanate NWs were formed by ion-exchange process without changing their morphology or crystal structure. The final calcination process led to the formation of the single-crystalline anatase TiO_2 NWs. This sequential process yielded 2–50 μm-long, single-crystalline NWs that oriented in the (100) direction and primarily normal to the Ti foil. The DSSCs fabricated using 12 μm-thick TiO_2 NW films on Ti foil showed a low-energy conversion efficiency ($\sim$1.4%), which was explained by five times lower roughness factor compared to the NP film and the formation of a thick, resistive TiO_2 layer between the NWs and Ti foil during the calcinations step. In a similar context, TiO_2 NWs were grown on a spiral-shaped titanium foil, synthesized by hydrothermal reactions at 230°C for 4 h to form NWs with diameters of 20–23 nm and lengths of 2–5 μm [78]. The TiO_2 NWs were randomly oriented and entangled to form a macroporous structured film. The TiO_2 NW film provided sufficient porosity for efficient dye adsorption and fast diffusion of redox couple. Accordingly, the DSSCs composed of TiO_2 NWs grown on the spiral-shaped titanium wire showed a conversion efficiency of 0.85% (V_{oc}: 0.616 V, J_{sc}: 2.3 mA/cm^2, FF: 0.61).

Furthermore, in a similar hydrothermal process using TiO_2 NPs as seeds, oriented TiO_2 NTs were formed on the Ti foil [79]. After the preparation of a dilute TiO_2 suspension by dispersing 1.0 g of Degussa P25 powder in deionized (DI) water, the TiO_2 NPs were deposited onto a Ti foil through dip coating in the suspension. The Ti foil containing the predeposited TiO_2 NPs reacted with an alkaline solution in a sealed Teflon® reactor containing 10 mL of 10 M NaOH solution. After reaction, the Ti foil, now covered with the newly formed film, was washed with DI water. The film showed an oriented texture and titanate structure composed of multilayered sheets.

Recently, single-crystalline rutile TiO_2 NRs or NWs were formed on FTO by adjusting parameters such as growth time, growth temperature, initial reactant concentration, acidity, and additives to control the diameters and lengths of the single-crystalline TiO_2 NRs [80]. The key factor in growing single- crystalline rutile TiO_2 NRs is a small lattice mismatch (epitaxial relation) between the FTO substrate and rutile TiO_2, driving the nucleation and growth of the nanorods. Figure 18 shows FE-SEM images of oriented, single crystal TiO_2 NWs on the FTO substrate. The entire surface of the FTO substrate is covered very uniformly with TiO_2 NRs with lengths of 90 $\pm$ 5 nm and diameters of 1.9 $\pm$ 0.1 μm. The NRs are nearly perpendicular to the FTO substrate. For application to DSSCs, an array of 4 μm-long TiO_2 NRs was used as the photoanode. To increase the dye adsorbing area, $TiCl_4$ treatment was carried out to give a photoconversion efficiency of 3% (V_{oc}: 0.71 V, J_{sc}: 6.05 mA/cm^2, FF: 0.7). However, the single-crystalline TiO_2 NWs didnot show any improvement in the electron dynamics relative to the TiO_2 NP systems due to the intrinsic properties of rutile TiO_2 [81] and a dependence on the slow and light intensity-dependent electron transport rate, indicating that trapping and detrapping, mostly in surface traps, still play an important role in electron transport [82]. Besides, a *c*-axis, highly oriented, sandwiched TiO_2 film was grown by hydrothermal process, in which one TiO_2 NP interlayer acted as the seed layer [83]. Two layers of TiO_2 NRs were grown toward both directions of the bulk solution and the substrate. Figure 19

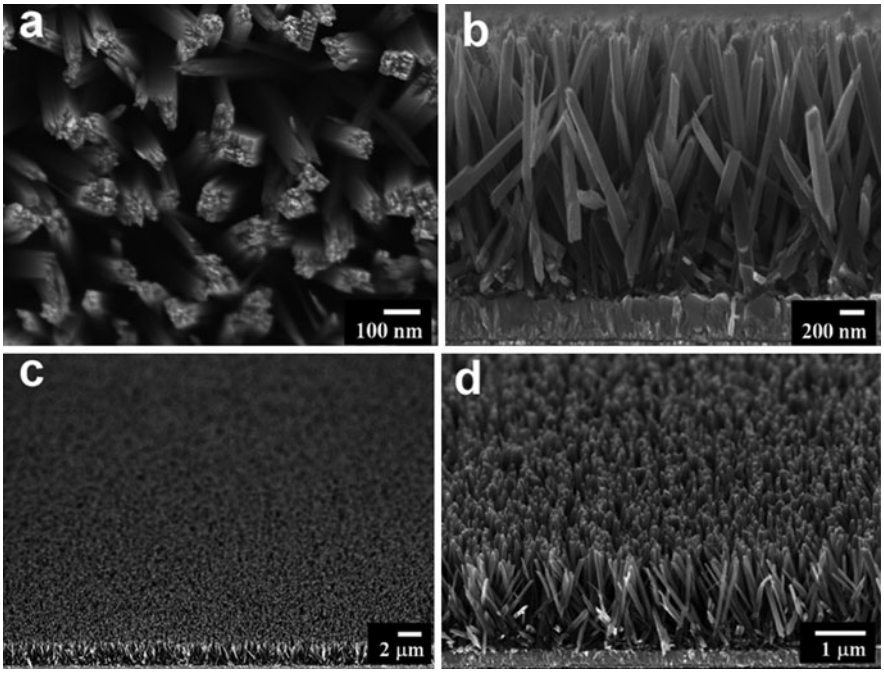

Fig. 18 FE-SEM images of oriented, rutile TiO_2 NR film grown on an FTO substrate at 150°C for 20 h: **a** top, **b** cross-sectional, and **c** and **d** tilted cross-sectional views (Reprinted with permission from Ref. [80]. Copyright 2009 American Chemical Society)

shows a schematic illustration of the formation mechanism of the sandwiched TiO_2 film. The high supersaturation degree of the solution leads to homogenous nucleation of TiO_2, which is precipitated on the FTO surface as seeds for further growth. From these seeds, subsequent crystal growth proceeds radially in the directions of the bulk solution and the substrate along with FTO etching. The density and length of the TiO_2 NRs can be tuned on both sides simply by controlling the reaction temperature and time.

Furthermore, Miyauchi et al. later reported a hydrothermal method for growing TiO_2 nanotubular arrays directly on the Ti substrate without the use of TiO_2 seeds [84]. The resultant nanotubular array structure exhibits superhydrophilic properties. Furthermore, the use of branched titanate NTs to grow a 3-D nanotubular network directly on the Ti substrate was reported [85]. The resultant 3-D nanotubular network exhibits a unique, three-dimensional, uniform, and porous structure. The 3-D nanotubular network structure was formed by the joining of branched NTs, as opposed to the previous vertical growth on the substrate. The inner and outer tubular diameters of the branched titanate NTs were approximately 6 and 12 nm, respectively. Branched titanate NTs were formed on the Ti substrate (Fig. 20). Therefore, a continuous seed formation-oriented, crystal growth mechanism was proposed for the branched titanate nanotubular network formation.

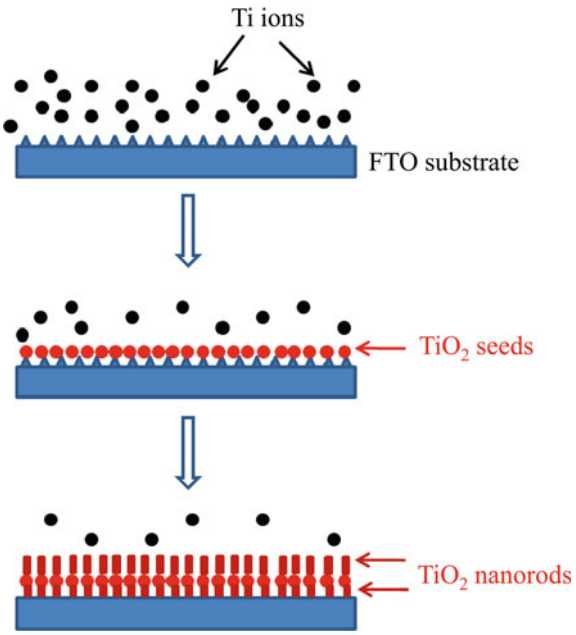

Fig. 19 Schematic illustration of the formation mechanism of sandwiched TiO_2 film: (I) formation of TiO_2 seeds, and (II) growth of TiO_2 NRs in both directions (Reprinted with permission from Ref. [83]. Copyright 2009 IOP Publishing Ltd.)

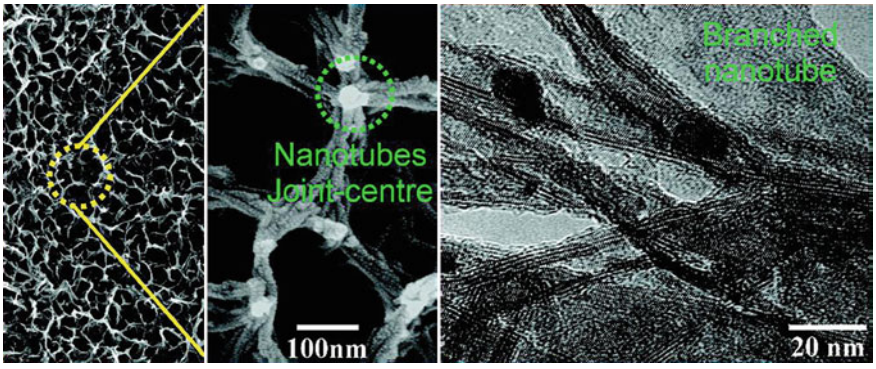

Fig. 20 FE-SEM and TEM images of hydrothermally prepared, nanobranched TiO_2 nanotubes (Reprinted with permission from Ref. [85]. Copyright 2010 American Chemical Society)

When implemented in a DSSC, this morphology produced a J_{sc} of 5.58 mA/cm^2, and V_{oc} of 0.74 V, and a FF of 60%. An overall photoconversion efficiency was 3.0%, compared to only 0.33% with a J_{sc} of 1.01 mA/cm^2, an V_{oc} of 0.65 V, and a FF of 0.42 for the DSSCs constructed using a TiO_2 porous film photoanode. From these results, the conversion efficiency of the 3-D titanate NT network photoanode cell was nine times higher than that of the TiO_2 porous film photoanode cell, which

was attributed to the textural and structural properties of the 3-D nanotubular network architecture.

4 Future Outlook

One of the challenges in the fabrication of highly efficient DSSCs is the control of the charge recombination that occurs in the interfacial region between the TiO_2 photoanode and dye/redox electrolyte. To overcome this problem, the use of a 1-D NR/NT photoanode instead of the previously applied NP film has been researched to increase the electron transport properties. Despite active investigations of various DSSC photoanodes from NPs to 1-D NR/NT, the electron dynamics remain comparable to those of the NP system. To further enhance the electron transport properties, four promising photoanode designs have been proposed: (1) single-crystalline TiO_2 NRs or NTs directly grown on the substrate will hinder charge recombination due to the fast electron transport rate, (2) the development of a self-assembly method to deposit the 1-D TiO_2 nanomaterials, (3) the use of single wall carbon NT scaffolds to increase the charge separation and transport, and (4) the fabrication of a core-shell structure with a core material showing fast electron transport rate, such as ZnO, Cu, Sn, Ti, and doped TiO_2, and a shell material mainly consisting of TiO_2 due to the consideration of the electronic bandgap. The significant enhancement of electron transport ability in the DSSC photoanode that is expected to be achieved from these research efforts will contribute to the blocking of photogenerated electron loss, and hence the improvement of photoconversion efficiency in the DSSCs.

Acknowledgment This work was supported by the Research Center for Energy Conversion and Storage (Contract No. R11-2002-102-00000-0) and the WCU (World Class University) program (R31-10013) through the National Research Foundation of Korea funded by the Ministry of Education, Science and Technology.

References

1. Bennett JM, Pelletier E, Albrand G et al (1989) Comparison of the properties of titanium dioxide films prepared by various techniques. Appl Opt 28:3303–3317
2. Wang TM, Zheng SK, Hao WC et al (2002) Studies on photocatalytic activity and transmittance spectra of TiO_2 thin films prepared by r.f. magnetron sputtering method. Surf Coat Technol 155:141–145
3. Manna L, Scher EC, Li L-S, Alivisatos AP (2002) Epitaxial growth and photochemical annealing of graded CdS/ZnS shells on colloidal CdSe nanorods. J Am Chem Soc 124:7136–7145
4. Nelson J (1987) Organic photovoltaic films. Curr Opin Solid State Mater Sci 6:87–95
5. Law M, Greene LE, Yang PD et al (2005) Nanowire dye-sensitized solar cells. Nat Mater 4:455–459
6. Naoi K, Ohko Y, Tatsuma T (2004) TiO_2 films loaded with silver nanoparticles: control of multicolor photochromic behavior. J Am Chem Soc 125:3664–3668

7. Yang Z, Xu T, Ito Y, Welp U et al (2009) Enhanced electron transport in dye-sensitized solar cells using short ZnO nanotips on a rough metal anode. J Phys Chem C 113:20521–20526
8. O'Regan B, Grätzel M (1991) A low-cost, high-efficiency solar cell based on dye-sensitized colloidal TiO_2 films. Nature 353:737–740
9. Wang Z-S, Kawauchi H, Kashima T, Arakawa H (2004) Significant influence of TiO_2 photoelectrode morphology on the energy conversion efficiency of N719 dye-sensitized solar cell. Coord Chem Rev 248:1381–1389
10. Kopidakis N, Benkstein KD, van de Lagemaat J, Frank AJ (2003) Transport-limited recombination of photocarriers in dye-sensitized nanocrystalline TiO_2 solar cells. J Phys Chem B 107:11307–11315
11. Solbrand A, Henningsson A, Södergren S, Lindström H, Hagfeldt A, Lindquist S-E (1999) Charge transport properties in dye-sensitized nanostructured TiO_2 thin film electrodes studied by photoinduced current transients. J Phys Chem B 103:1078–1083
12. You M, Kim TG, Sung Y-M (2010) Synthesis of Cu-doped TiO_2 nanorods with various aspect ratios and dopant concentrations. Cryst Growth Des 10:983–987
13. Pradhan SK, Reucroft PJ, Yang F, Dozier A (2003) Growth of TiO_2 nanorods by metalorganic chemical vapor deposition. J Cryst Growth 256:83–88
14. Lei Y, Zhang LD, Meng GW et al (2001) Preparation and photoluminescence of highly ordered TiO_2 nanowire arrays. Appl Phys Lett 78:1125–1127
15. Wolcott A, Smith WA, Kuykendall TR et al (2009) Photoelectrochemical water splitting using dense and aligned TiO_2 nanorod arrays. Small 5:104–111
16. Polleux J, Pinna N, Niederberger M (2005) Ligand functionality as a versatile tool to control the assembly behavior of preformed titania nanocrystals. Chem Eur J 11:3541–3551
17. Cozzoli PD, Kornowski A, Weller H (2003) Low-temperature synthesis of soluble and processable organic-capped anatase TiO_2 nanorods. J Am Chem Soc 125:14539–14548
18. Schubert U, Tewinkel S, Lamber R (1996) Metal complexes in inorganic matrixes. 15. Coordination of metal ions by lysinate-modified titanium and zirconium alkoxides and the preparation of metal/titania and metal/zirconia nanocomposites. Chem Mater 8:2047–2055
19. Jiu J, Isoda S, Wang F, Adachi M (2006) Dye-sensitized solar cells based on a single-crystalline TiO_2 nanorod film. J Phys Chem B 110:2087–2092
20. Penn RL, Banfield JF (1998) Imperfect oriented attachment: dislocation generation in defect-free nanocrystals. Science 281:969–971
21. Penn RL, Banfield JF (1999) Morphology development and crystal growth in nanocrystalline aggregates under hydrothermal conditions: insights from titania. Geochim Cosmochim Acta 63:1549–1557
22. Penn RL (2004) Kinetics of oriented aggregation. J Phys Chem B 108:12707–12712
23. Han S, Choi S-H, Hyeon T et al (2005) Low-temperature synthesis of highly crystalline TiO_2 nanocrystals and their application to photocatalysis. Small 1:812–816
24. Kang SH, Choi S-H, Hyeon T, Sung Y-E (2008) Nanorod-based dye-sensitized solar cells with improved charge collection efficiency. Adv Mater 20:54–58
25. Nakade S, Kanzaki T, Yanagida S et al (2005) Stepped light-induced transient measurements of photocurrent and voltage in dye-sensitized solar cells: application for highly viscous electrolyte systems. Langmuir 21:10803–10807
26. Fisher AC, Peter LM, Ponomarev EA et al (2000) Intensity dependence of the back reaction and transport of electrons in dye-sensitized nanocrystalline TiO_2 solar cells. J Phys Chem B 104:949–958
27. Bisquert J, Zaban A, Salvador P (2002) Analysis of the mechanisms of electron recombination in nanoporous TiO_2 dye-sensitized solar cells. Nonequilibrium steady-state statistics and interfacial electron transfer via surface states. J Phys Chem B 106:8774–8782
28. Usami A, Ozaki H (2001) Computer simulations of charge transport in dye-sensitized nanocrystalline photovoltaic cells. J Phys Chem B 105:4577–4583
29. Adachi M, Murata Y et al (2004) Highly efficient dye-sensitized solar cells with a titania thin-film electrode composed of a network structure of single-crystal-like TiO_2nanowires made by the "oriented attachment" mechanism. J Am Chem Soc 126:14943–14949

30. Li S, Li Y, Wang H et al (2009) Peptization-hydrothermal method as a surfactant-free process toward nanorod-like anatase TiO_2 nanocrystals. Eur J Inorg Chem 2009:4078–4084
31. Brinker CJ, Schere GW (1989) Sol-gel science: the physics and chemistry of sol-gel processing. Elsevier Science, USA
32. Chemseddine A, Moritz T (1999) Nanostructuring titania: control over nanocrystal structure, size, shape, and organization. Eur J Inorg Chem 1999:235–245
33. Kasuga T, Hiramatsu M, Hoson A et al (1999) Titania nanotubes prepared by chemical processing. Adv Mater 11:1307–1311
34. Ohsaki Y, Masaki N, Yanagida S et al (2005) Dye-sensitized TiO_2 nanotube solar cells: fabrication and electronic characterization. Phys Chem Chem Phys 7:4157–4163
35. Koo B, Park J, Hyeon T et al (2006) Simultaneous phase- and size-controlled synthesis of TiO_2 nanorods via non-hydrolytic sol-gel reaction of syringe pump delivered precursors. J Phys Chem B 110:24318–24323
36. Cheng H, Ma J, Qi L et al (1995) Hydrothermal preparation of uniform nanosize rutile and anatase particles. Chem Mater 7:663–671
37. Matthews A (1976) The crystallisation of anatase and rutile from amorphous titanium dioxide under hydrothermal conditions. Am Mineral 61:419–424
38. Izumi F (1978) The polymorphic crystallization of Titanium(IV) oxide under hydro-thermal conditions II. The roles of inorganic anions in the nucleation of rutile and anatase from acid solutions. Bull Chem Soc Jpn 51:1771–1776
39. Matijevic E (1977) The role of chemical complexing in the formation and stability of colloidal dispersions. J Colloid Interface Sci 58:374–389
40. Wei M, Konishi Y, Zhou H, Arakawa H et al (2006) Utilization of titanate nanotubes as an electrode material in dye-sensitized solar cells. J Electrochem Soc 153:A1232–A1236
41. Chen A, Zhou W, Du G, Peng L-M (2002) Trititanate nanotubes made via a single alkali treatment. Adv Mater 14:1208–1211
42. Boercker JE, Enache-Pommer E, Adyil ES (2008) Growth mechanism of titanium dioxide nanowires for dye-sensitized solar cells. Nanotechnology 19:095604–095613
43. Enache-Pommer E, Boercker JE, Adyil ES (2007) Electron transport and recombination in polycrystalline TiO_2nanowire dye-sensitized solar cells. Appl Phys Lett 91:123116–123118
44. Tan B, Wu Y (2006) Dye-sensitized solar cells based on anatase TiO_2 nanoparticle/nanowire composites. J Phys Chem B 110:15932–15938
45. Beppu T, Yamaguchi S, Hayase S (2007) Improvement of heat resistant properties of TiO_2 nanowires and application to dye-sensitized solar cells. Jpn J Appl Phys 46:4307–4311
46. Oh J-K, Lee J-K, Park K-W (2010) TiO_2 branched nanostructure electrodes synthesized by seeding method for dye-sensitized solar cells. Chem Mater 22:1114–1118
47. Meekins BH, Kamat PV (2009) Got TiO_2 nanotubes lithium ion intercalation can boost their photoelectrochemical performance. ACS Nano 3:3437–3446
48. Kuang D, Brillet J, Chen P, Grätzel M et al (2008) Application of highly ordered TiO_2 nanotube arrays in flexible dye-sensitized solar cells. ACS Nano 2:1113–1116
49. Shankar K, Mor GK, Prakasam HE, Grimes CA (2007) Self-assembled hybrid polymer-TiO_2 nanotube array heterojunction solar cells. Langmuir 23:12445–12449
50. Yu B-Y, Tsai A, Tsai S-P, Wong K-T, Shyue J-J (2008) Efficient inverted solar cells using TiO_2 nanotube arrays. Nanotechnology 19:255202–255206
51. Wang J, Lin Z (2010) Dye-sensitized TiO_2 nanotube solar cells with markedly enhanced performance via rational surface engineering. Chem Mater 22:579–584
52. Zwilling V, Aucouturier M, Darque-Ceretti E (1999) Anodic oxidation of titanium and TA6 V alloy in chromic media. An electrochemical approach. Electrochim Acta 45:921–929
53. Macäk JM, Tsuchiya H, Schmuki P (2005) High-aspect-ratio TiO_2 nanotubes by anodization of titanium. Angew Chem Int Ed 44:2100–2102
54. Cai QPM, Varghese OK, Grimes CA et al (2005) The effect of electrolyte composition on the fabrication of self-organized titanium oxide nanotube arrays by anodic oxidation. J Mater Res 20:230–236

55. Taveira LV, Macäk JM, Tsuchiya H, Schmuki P et al (2005) Initiation and growth of self-organized TiO_2 nanotubes anodically formed in $NH_4F/(NH_4)_2SO_4$ electrolytes. J Electrochem Soc 152:B405–B410
56. Kang SH, Kim J-Y, Sung Y-E et al (2008) Formation and mechanistic study of self-ordered TiO_2 nanotubes on Ti substrate. J Ind Eng Chem 14:52–59
57. Bayoumi FM, Ateya BG (2006) Formation of self-organized titania nano-tubes by dealloying and anodic oxidation. Electrochem Comm 8:38–44
58. Paulose M, Shankar K, Varghese OK, Grimes CA et al (2006) Backside illuminated dye-sensitized solar cells based on titania nanotube array electrodes. Nanotechnology 17:1446–1448
59. Hahn R, Stergiopoulus T, Schmuki P et al (2007) Efficient solar energy conversion using TiO_2 nanotubes produced by rapid breakdown anodization—a comparison. Phys Stat Sol (RRL) 1:135–137
60. Kang SH, Kim J-Y, Sung Y-E et al (2007) Surface modification of stretched TiO_2 nanotubes for solid-state dye-sensitized solar cells. J Phys Chem C 111:9614–9623
61. Bisquert J, Zaban A, Greenshtein M, Mora-Seró I (2004) Determination of rate constants for charge transfer and the distribution of semiconductor and electrolyte electronic energy levels in dye-sensitized solar cells by open-circuit photovoltage decay method. J Am Chem Soc 126:13550–13559
62. Fabregat-Santiago F, García-Cañadas J (2004) The origin of slow electron recombination processes in dye-sensitized solar cells with alumina barrier coatings. J Appl Phys 96:6903–6907
63. Macak JM, Tsuchiya H, Schmuki P et al (2005) Smooth anodic TiO_2 nanotubes. Angew Chem Int Ed 44:7463–7465
64. Shankar K, Mor GK, Grimes CA et al (2007) Highly-ordered TiO_2 nanotube arrays up to 220 μm in length: use in water photoelectrolysis and dye-sensitized solar cells. Nanotechnology 18:065707–065717
65. Paulose M, Shankar K, Yoriya S, Grimes CA et al (2006) Anodic growth of highly ordered TiO_2 nanotube arrays to 134 μm in length. J Phys Chem B 110:16179–16184
66. Lee W, Kang SH, Sung Y-E, Han S-H et al (2008) Co-sensitization of vertically aligned TiO_2 nanotubes with two different sizes of CdSe quantum dots for broad spectrum. Electrochem Comm 10:1579–1582
67. Wang J, Lin Z (2008) Freestanding TiO_2 nanotube arrays with ultrahigh aspect ratio via electrochemical anodization. Chem Mater 20:1257–1261
68. Zhu K, Neale NR, Frank AJ et al (2007) Enhanced charge-collection efficiencies and light scattering in dye-sensitized solar cells using oriented TiO_2 nanotubes arrays. Nano Lett 7:69–74
69. Kang SH, Kim HS, Sung Y-E et al (2009) An investigation on electron behavior employing vertically-aligned TiO_2 nanotube electrodes for dye-sensitized solar cells. Nanotechnology 20:355307–355312
70. Kim D, Ghicov A, Schmuki P et al (2008) Bamboo-type TiO_2 nanotubes: improved conversion efficiency in dye-sensitized solar cells. J Am Chem Soc 130:16454–16455
71. Zhu K, Neale NR, Frank AJ et al (2007) Removing structural disorder from oriented TiO_2 nanotube arrays: reducing the dimensionality of transport and recombination in dye-sensitized solar cells. Nano Lett 7:3739–3746
72. Roy P, Kim D, Schmuki P et al (2009) Improved efficiency of TiO_2 nanotubes in dye sensitized solar cells by decoration with TiO_2 nanoparticles. Electrochem Comm 11:1001–1004
73. Park H, Yang D-J, Kim H-G et al (2009) Fabrication of MgO-coated TiO_2 nanotubes and application to dye-sensitized solar cells. J Electroceram 23:146–149
74. Ito S, Cevey Ha N-L, Grätzel M et al. (2006) High-efficiency (7.2%) flexible dye-sensitized solar cells with Ti-metal substrate for nanocrystalline-TiO_2 photoanode. Chem Comm 4004–4006

75. Mor GK, Shankar K, Paulose M, Grimes CA et al (2006) Use of highly-ordered TiO_2 nanotube arrays in dye-sensitized solar cells. Nano Lett 6:215–218
76. Varghese OK, Paulose M, Grimes CA (2009) Long vertically aligned titania nanotubes on transparent conducting oxide for highly efficient solar cells. Nat Mater 4:592–597
77. Liu B, Boercker JE, Aydil ES (2008) Oriented single crystalline titanium dioxide nanowires. Nanotechnology 19:505604–505610
78. Wang H, Liu Y, Li M et al (2009) Hydrothermal growth of large-scale macroporous TiO_2 nanowires and its application in 3D dye-sensitized solar cells. Appl Phys A 97:25–29
79. Tian ZR, Voigt JA, Xu H et al (2003) Large oriented arrays and continuous films of TiO_2-based nanotubes. J Am Chem Soc 125:12384–12385
80. Liu B, Adyil ES (2009) Growth of oriented single-crystalline rutile TiO_2 nanorods on transparent conducting substrates for dye-sensitized solar cells. J Am Chem Soc 131:3985–3990
81. Kang SH, Kang M-S, Sung Y-E et al (2008) Columnar rutile TiO_2 based dye-sensitized solar cells by radio-frequency magnetron sputtering. J Power Sources 184:331–335
82. Enache-Pommer E, Liu B, Adyil ES (2009) Electron transport and recombination in dye-sensitized solar cells made from single-crystal rutile TiO_2 nanowires. Phys Chem Chem Phys 11:9648–9652
83. Han Y, Wu G, Wang M, Chen H (2009) The growth of a *c*-axis highly oriented sandwiched TiO_2 film with superhydrophilic properties without UV irradiation on SnO:F substrate. Nanotechnology 20:235605–235611
84. Miyauchi M, Tokudome H (2007) Super-hydrophilic and transparent thin films of TiO_2 nanotube arrays by a hydrothermal reaction. J Mater Chem 17:2095–2100
85. Zhang H, Liu P, Zhao H et al (2010) Facile formation of branched titanate nanotubes to grow a three-dimensional nanotubular network directly on a solid substrate. Langmuir 26:1574–1578